

MIGRATION AND DYNAMICAL RELAXATION IN CROWDED SYSTEMS OF GIANT PLANETS

Fred C. Adams^{1,2} and Gregory Laughlin³

¹*Michigan Center for Theoretical Physics*

Physics Department, University of Michigan, Ann Arbor, MI 48109

²*Astronomy Department, University of Michigan, Ann Arbor, MI 48109*

³*Lick Observatory, University of California, Santa Cruz, CA 95064*

ABSTRACT

This paper explores the intermediate-time dynamics of newly formed solar systems with a focus on possible mechanisms for planetary migration. We consider two limiting corners of the available parameter space – crowded systems containing $\mathcal{N} = 10$ giant planets in the outer solar system, and solar systems with $\mathcal{N} = 2$ planets that are tidally interacting with a circumstellar disk. Crowded planetary systems can be formed in accumulation scenarios – if the disk is metal rich and has large mass – and through gravitational instabilities. The planetary system adjusts itself toward stability by spreading out, ejecting planets, and sending bodies into the central star. For a given set of initial conditions, dynamical relaxation leads to a well-defined distribution of possible solar systems. For each class of initial conditions, we perform large numbers (hundreds to thousands) of N-body simulations to obtain a statistical description of the possible outcomes. For $\mathcal{N} = 10$ planet systems, we consider several different planetary mass distributions; we also perform secondary sets of simulations to explore chaotic behavior and longer term dynamical evolution. For systems with 10 planets initially populating the radial range $5 \text{ AU} \leq a \leq 30 \text{ AU}$, these scattering processes naturally produce planetary orbits with $a \sim 1 \text{ AU}$ and the full range of possible eccentricity ($0 \leq \epsilon \leq 1$). Shorter period orbits (smaller a) are difficult to achieve. To account for the observed eccentric giant planets, we also explore a mechanism that combines dynamical scattering and tidal interactions with a circumstellar disk. This combined model naturally produces the observed range of semi-major axis a and eccentricity ϵ . We discuss the relative merits of the different migration mechanisms for producing the observed eccentric giant planets.

Keywords: Extrasolar planets – planetary dynamics – planetary formation

1. INTRODUCTION

The past decade has witnessed a revolution in the study of planetary systems, with over one hundred extrasolar planets discovered thus far. The initial discoveries (Mayor and Queloz 1995; Marcy and Butler 1996) showed an unexpected feature – namely that the orbital parameters of the newly discovered planets were markedly different from those of the planets in our solar system. Many of the giant planets are found in short period orbits ($P_{\text{orb}} \approx 4$ days) while others display longer orbits of high eccentricity ($0 \leq \epsilon \leq 0.92$). Subsequent discoveries (e.g., Marcy and Butler 1998, 2000; Hatzes et al. 2000; Perryman 2000) have shown that such planetary systems are relatively common. Approximately 8 percent of the stars in the solar neighborhood have giant planets in tight orbits with $a < 3$ AU. Hot Jupiters – giant planets in ~ 4 day orbits – account for one eighth of the observed sample of planets (1 percent of the stars). The remaining seven eighths of the observational sample (7 percent of the stars) have eccentric giant planets. This observed population of planets shows an apparent deficit of orbits with periods P in the range $10 < P < 100$ days. If this observational trend holds up, it may suggest that different migration (or formation) mechanisms are at work for the hot Jupiters ($P \sim 4$ days) and the eccentric giants ($P \geq 100$ days). In any case, an explanation for the origin of these orbits poses an important astronomical problem.

Theories of planet formation come in two main varieties. The leading theory, at least for our own solar system, holds that planets form “from the bottom up” through the gradual accumulation of planetessimals (see the review of Lissauer 1993). These rocky building blocks collect into larger entities until their gravitational influence is strong enough to accrete gas from the surrounding nebula. In circumstellar disks with sufficiently high mass, the ascent from planetessimals to giant planets can occur rapidly and can lead to crowded systems (Lissauer 1987; Lin and Ida 1997; see also Levison, Lissauer, and Duncan 1998). The majority of the newly discovered planetary systems orbit stars with high metallicity (e.g., Gonzalez 1997, Laughlin 2000), which supports the production of more rocky material and enhances the rapid assembly of giant planets. The alternate theory holds that planets form “from the top down” through the action of gravitational instabilities in the circumstellar disk (e.g., Cameron 1978; Boss 2000). Under ideal conditions, gravitational instabilities can grow on a time scale comparable to the orbital period of the outer disk edge (Adams, Ruden, and Shu 1989). For disks with radius $r_{\text{disk}} \approx 30$ AU, for example, the instability time scale is thousands of years, much shorter than the relaxation time of the system (see below). As a result, giant planet formation can occur even more rapidly through this channel.

In both scenarios outlined above, planet formation can proceed – at least in principle – faster than dynamical relaxation of the newly formed system. The initial states for the planetary systems are not, in general, dynamically stable over much longer time intervals. The astronomical motivation for this present study is to explore the dynamics of these crowded planetary systems in greater detail. In particular, we can find the odds of obtaining high eccentricity planets with $a \sim 1$ AU (like many of those observed).

This study has another objective. Solar system formation is likely to be chaotic – in the

technical sense. Due to sensitive dependence on the starting conditions, the result of any particular realization of solar system formation cannot be described in terms of a single outcome. Instead, a set of physically equivalent starting conditions will generally display a full distribution of outcomes. In this study, we illustrate this behavior explicitly by calculating the distribution of outcomes for each chosen set of initial conditions.

In addition to the astronomical applications, this study provides an interesting problem in dynamics. These planetary systems have their gravitational potential dominated by the central star and they begin with their primary motions as orbits about the central mass. As a result, the relaxation of a planetary system will be somewhat different from that of a stellar system (such as a globular cluster – see Binney and Tremaine 1987).

This research builds on previous work. Dynamical instabilities involving two giant planets have been explored extensively through numerical simulations (Ford, Havlickova, and Rasio 2001). This work showed that interactions between only two planets (with equal mass) cannot reproduce the orbital characteristics of the observed extrasolar planets (see also Rasio and Ford 1996; Weidenschilling and Marzari 1996); similarly, a single close encounter between two planets cannot explain the observed orbits (Katz 1997). A more recent study considers dynamical instabilities involving three Jupiter-mass planets (Marzari and Weidenschilling 2002) and compares favorably with the observations (see also Ford, Radio, and Yu 2002 for the case of unequal mass planets). Dynamical relaxation in larger systems of extrasolar planets has been considered by Papaloizou and Terquem (2001; see also Terquem and Papaloizou 2002; Lin and Ida 1997; Chambers, Wetherill, and Boss 1996). As noted by many previous authors, the parameter space available to multiple planet solar systems is enormous. The dynamical relaxation portion of this study extends previous work by providing a systematic exploration of one region of parameter space – that containing $\mathcal{N} = 10$ planets within 30 AU of the central star. In order to obtain statistically meaningful results, this work employs many realizations (typically, $N = 100$) of any given starting condition and determines the distribution of possible outcomes.

Many previous authors have also considered tidal torques exerted on planets by circumstellar disks. Migration was anticipated long before extrasolar planets were detected (e.g., Goldreich and Tremaine 1980; Lin and Papaloizou 1993). With the discovery of extrasolar planets in short period orbits, many studies of migration have been carried out (e.g., Lin, Bodenheimer, and Richardson 1996; Trilling et al. 1998; Nelson et al. 2000). These studies generally consider only one planet at a time; however, two planet systems have recently been considered (Lee and Peale 2002; Murray, Paskowitz, and Holman 2002). In this work, we extend these calculations to include instabilities between multiple planets in the presence of tidal torques from a surrounding disk. The simultaneous action of both dynamical scattering and viscous torquing allows for a wider variety of behavior and final system properties. The tidal torques are efficient at moving planets inward, while the scattering interactions are effective at increasing orbital eccentricity. The combination naturally produces planetary orbits with small semi-major axis a and large eccentricity ϵ , much like some of the observed eccentric giant planets.

This paper is organized as follows. In §2, we describe the numerical treatment and the collections of initial conditions used for the both the dynamical relaxation experiments and the disk-torquing simulations. The basic dynamical results are presented in §3, including a specification of the distributions of final system properties. We also demonstrate the chaotic nature of the dynamics and find the dependence of the time scales on the planetary masses and other parameters of the problem. In §4, we present a complementary set of simulations that include scattering of only two planets, but include the tidal interaction of the outer planet with a circumstellar disk. We conclude with a summary and discussion of our results in §5.

2. METHODS AND INITIAL CONDITIONS

The focus of this investigation is to perform numerical simulations of nascent planetary systems. The numerical experiments were carried out by using the *Mercury 6* integration package (Chambers 1999), which provides general-purpose software for N-body integrations. Since the code was designed to calculate the orbital evolution of objects moving in the gravitational field of a central star, it is well-suited for this purpose. In order to maintain sufficient accuracy, we use the Bulirsch-Stoer (BS) integration scheme for all of the simulations presented herein. Although somewhat slower than other computational options, the BS scheme maintains greater accuracy during close encounters, which drive the evolution of these planetary systems. Specifically, we use an integration accuracy parameter of 10^{-11} which sets the maximum fractional error per time step. For the course of one million years integrations (see below), the accumulated fractional error in the energy $\Delta E/E$ is typically a few parts per million. Angular momentum is conserved to greater accuracy, with a typical fractional error in $\Delta J/J$ of only a few parts per billion.

In the first phase of this investigation, we set up a series of simulations with the following properties. Each system begins with $\mathcal{N} = 10$ planets orbiting a star with mass $M_* = 1.0 M_\odot$. We perform four ensembles of $N = 100$ simulations, where each set uses a particular distribution to specify the planetary masses (see below). At the start of each simulation, the planets are placed on circular orbits, with the logarithm of the orbital radius chosen randomly over the range corresponding to $5 \text{ AU} \leq r \leq 30 \text{ AU}$ (the range of semi-major axes sampled by giant planets in our solar system). The initial velocities are chosen to be those appropriate for circular orbits at the given radius. The angular location of the planets is random. Furthermore, the planets are displaced above or below the orbital plane by a small amount, a randomly chosen distance between zero and a “scale height” defined to be $H = 0.05r$. With this set of initial conditions, the planets are then integrated for a time interval of one million years.

For our four initial ensembles of simulations, we adopt the following mass distributions: [A] All 10 planets have equal mass, where $m_P = m_J = 0.001 M_\odot$. [B] All 10 planets have equal mass, where $m_P = 2m_J = 0.002 M_\odot$. [C] The 10 planets have masses drawn from a random (uniform) distribution over the mass range $0 \leq m_P \leq 4m_J = 0.004 M_\odot$. [D] The 10 planets have masses that are uniformly distributed in $\log m$ and are chosen from the range $-1 \leq \log_{10}[m_P/m_J] \leq 1$. In

all cases, the planetary masses are drawn independently. For each mass distribution, we perform $N = 100$ separate numerical integrations ($N=100$ different realizations of the same class of initial conditions). The resulting ensembles of solar systems (100 for each mass distribution) can be characterized in a statistically significant manner. For the two of the mass distributions (the uniform random and logarithmic random cases), we follow up these initial numerical experiments with a smaller number ($N = 25$) of longer term integrations. Finally, we consider another mass distribution that contains one high mass planet ($m_P = m_J$) and 19 smaller planets with mass in the range $0 \leq m_P \leq 0.5 m_J$ (see §3.5).

In this initial set of simulations, we ignore the possibility of planets merging. For two planet systems, the effects of merging have been clearly delineated (Ford et al. 2001). When the parameter $b_M \equiv (r_P/r_J)(a/5\text{AU})^{-1}$ is less than unity, collisions between planets are relatively unimportant (see Fig. 7 of Ford et al. 2001). As a result, if the planets have merging cross sections that are comparable to the physical size of present-day giant planets, merging can be safely neglected for the regime of parameter space sampled by our simulations. As a benchmark, in §4 we consider tidal torques acting on pairs of planets, which migrate inwards to small semi-major axes; collisions are included in these simulations, where the effective planetary radius $r_P \approx 2r_J$. The results of §4 show that collisions take place in less than 2 percent of the systems and that the merging planets typically have radial locations $r \sim 1 - 3$ AU. Furthermore, the results of §3 show that when planets are scattered inward to $a \sim 1$ AU, they are typically well isolated, with the semi-major axis of the next closest planet a factor of 15 – 20 farther larger. If the planets form through gravitational instability, however, the cross sections can be much larger and merging can become significant (see, e.g., Lin and Ida 1997). Notice also that in the absence of collisions, we could rescale our simulations to study starting conditions inside our chosen boundary at 5 AU. With $r_P \sim r_J$, we can only rescale the inner boundary to about 1 AU before collisions start to become important.

In §4, we consider smaller systems with only two planets, but allow the outer planet to be acted upon by an external torque from a surrounding circumstellar disk. These integrations are carried out using a BS scheme adopted from codes developed previously to study solar system scattering cross sections (Laughlin and Adams 2000; Adams and Laughlin 2001). This code is supplemented with subroutines from the Mercury 6 integration package (Chambers 1999). By using a code that is explicitly optimized for the few-body problem in the main integration, in conjunction with separately optimized subroutines for evaluating orbital elements, the code maintains both high accuracy and high speed. As before, we perform a large number (hundreds) of realizations of the problem to obtain a good determination of the distributions of possible outcomes.

3. RESULTS

For each of the four distributions outlined above, we perform $N = 100$ simulations and use the results to define the characteristic time scales (§3.1) and build up a statistical description of the outcomes (§3.2). We are particularly interested in the properties of the innermost surviving planets

in these systems (§3.3), as these survivors may explain the observed eccentric giant planets in the observational sample. With these results in hand, we also perform secondary sets of simulations to explore particular dynamical issues, including the chaotic nature of the dynamics (§3.4), scattering into resonant configurations (§3.5), the longer term dynamical evolution of the systems (§3.6), and more extreme planetary mass distributions – the action of many small planets on one large planet (also §3.6).

3.1. Time Scales

Crowded planetary systems, and the numerical simulations presented herein, display two important time scales. The first is the decay time, which is the time required for a solar system to decay by either ejecting a planet or sending a planet into the central star. The second time scale is the evolution time, i.e., the time over which the solar system adjusts itself to stability.

The statistics of solar system decay can be considered analogous to that used to describe the decay of atomic nuclei. The systems start with 10 planets and then decay into daughter systems with 9 planets. In this context, the decay has two channels, either outright ejection or accretion of the planet by the central star. In this context, we consider both channels to be different modes of the same effect. In the simplest case, the decay of an ensemble of systems follows the well known law $N(t) = N_0 \exp[-\Gamma t]$. A collection of solar system should follow such a law whenever the probability of decay (planetary ejection or accretion) is constant in time. As shown in Fig. 1, the four ensembles of this paper come close to following an exponential law. Nonetheless, the numerical results depart from purely exponential behavior when the number $N(t)$ of surviving systems is small.

This trend can be quantified. If we assume that the basic decay law has an exponential form, then at any given time each solar system has a probability $q = e^{-\Gamma t}$ of surviving and a probability $p = 1 - q$ of having already decayed. The distribution of surviving (undecayed) systems thus has a binomial form

$$P(n) = \sum_{n=0}^N C_{Nn} q^n p^{N-n}, \quad (1)$$

where N is the total number of systems (100) and n is the number of solar systems surviving to time t . From this distribution, we can calculate the expectation value $\langle n \rangle = qN$, the second moment $\langle n^2 \rangle = q^2 N(N - 1) + qN$, and the width of the distribution $\sigma = [q(1 - q)N]^{1/2}$. As expected, the relative width of the distribution grows larger as the number $N(t)$ of surviving systems decreases. In particular, a measure of the relative width can be written in the form

$$\frac{\sigma}{\langle n \rangle} = \left(\frac{1 - q}{qN} \right)^{1/2} = N^{-1/2} [e^{\Gamma t} - 1]^{1/2}. \quad (2)$$

To estimate the decay time scale, we fit a straight line to the semi-log curves in Fig. 1. The

fitting procedure is weighted by the errors in the data and Eq. [2] is employed to estimate the errors (due to the ever shrinking sample size). The slope of the fitted line determines the value of Γ , which in turn defines the exponential decay time $\tau_{\text{decay}} \equiv \Gamma^{-1}$. The resulting time scales are listed in Table I for the four ensembles of solar systems. Because of the weighted fitting procedure, the straight line fits agree much better with the numerical results at shorter times; this behavior is due to the larger uncertainties that arise for longer decay times (due to small N statistics). For all four planetary mass distributions, the formal uncertainties in the half-lives are somewhat less than 2 percent. The decay time scales, as defined here, are relatively short, only 20,000 – 125,000 years. The half-life – the time required for half of the systems in the ensemble to decay – is related to the decay time via $\tau_{1/2} = \tau_{\text{decay}}(\ln 2)$.

The temporal evolution of these systems can be understood in terms of a dynamical relaxation process. For a wide variety of assumptions, the dynamical relaxation time scale can be written in the general form

$$\tau_R = P_{\text{orb}} Q \left(\frac{M_\star}{m_P} \right)^2, \quad (3)$$

where P_{orb} is the orbital period for a representative orbit, M_\star is the mass of the central star, m_P is the mass of the planets, and Q is a dimensionless factor that depends on the geometry, density, and other characteristics of the system. For example, the factor Q depends on whether the system is spherical or nearly planar, and can also include a logarithmic correction factor (e.g., see Binney and Tremaine 1987; Papaloizou and Terquem 2001).

For systems with equal mass planets, Eq. [3] predicts that the relaxation time scale should vary as the inverse square of the planetary masses. Indeed, the ensemble with $m_P = 1m_J$ has a decay time that is four times longer than that of the ensemble with $m_P = 2m_J$. The third ensemble, with a random distribution of masses with mean mass $2m_J$, has a somewhat shorter decay time. This result also makes sense: The planets that are ejected are generally the lower mass planets, which scatter off larger ones. So even though the mean planet mass is $2m_J$, the mean mass of the scatterers is higher and the time scale is correspondingly lower.

The decay time (or, equivalently, the half-life) defined above describes how the initial ensemble of solar systems decays by removing a planet. The resulting daughter products continue to eject or accrete planets over longer time spans and we need to account for this continued evolution. To describe the longer term evolution, we consider the entire ensemble of $N = 100$ solar systems at once (for each given mass function of planets). This initial collection of 1000 planets is reduced over time, as calculated from the results of the suite of numerical simulations. By dividing the number of surviving planets by $N = 100$, we obtain an estimate of the “typical” evolution of a solar system over its first 1 Myr, i.e., an estimate of the function $\mathcal{N}(t)$. The results are shown in Fig. 2 for the four ensembles of this paper.

The initial decay time τ_{decay} is well defined because we start the entire ensemble of solar systems in equivalent – and known – initial states. The longer term evolution of the planetary systems is more complicated. After a solar system decays by losing a planet, the remaining daughter solar

system will be more spread out (and hence Q will change in Eq. [3]). To model this complication, we consider the relaxation time to take the form $t_R \propto \mathcal{N}^{-\beta}$, so that dynamical relaxation – and hence planetary ejection – takes longer as the number of planets decreases (again, see Binney and Tremaine 1987; Papaloizou and Terquem 2001). This form for the relaxation time implies that the number of planets as a function of time can be written in the form

$$\mathcal{N}(t) = \frac{\mathcal{N}_0}{[1 + \gamma t]^\alpha}, \quad (4)$$

where $\mathcal{N}_0 = 10$ (for these simulations), $\alpha = \beta^{-1}$, and where γ is determined by the magnitude of the relaxation time. For each evolution function $\mathcal{N}(t)$ shown in Fig. 2, we fit the results to a function of the form [4]. The resulting fits are shown as the solid curves in Fig. 2 and the values of γ and α are listed in Table I. Also listed in Table I is the evolution time scale τ_{evolve} , which is defined to be the time required (on average) for the number of planets in a solar system to be reduced by a factor of 2 (from $\mathcal{N} = 10$ to 5).

Table I shows that the decay time τ_{decay} or half-life $\tau_{1/2}$ is closely related to the evolution time τ_{evolve} . For each of the four ensembles of solar systems, the ratio of time scales $\mathcal{R} = \tau_{\text{evolve}}/\tau_{1/2}$ has a nearly constant value of $\mathcal{R} = 12 \pm 1$. In other words, for these ensembles of 10 planet systems, the time required for a solar system to lose half of its planets (the evolution time) is about 12 times longer than the time required for half of the population of solar systems to decay by losing its first planet (the half-life). Keep in mind that the half-life, as defined here, is the half-life of the initial 10 planet systems; the daughter products will contain fewer planets and have different (generally longer) half-lives.

(Table I: Characteristic Time Scales)

3.2. Properties of the Resulting Solar Systems

Another result of this set of simulations is the distributions of “final” solar system properties. Since the first portion of this study is limited to integrations of 1 Myr, the final solar system properties are those at the 1 Myr mark. Solar systems can continue to evolve over ever longer time frames – even the planets in our own (relatively sedate) solar system can change their orbital elements over sufficiently long time periods (e.g., Laskar 1990; Duncan and Quinn 1993). At the end of these 1 Myr integrations, the solar systems have undergone substantial dynamical evolution from their initial states and the suite of solar system properties is well defined.

For each simulation, we obtain the orbital elements of each surviving planet at the end of one million years. We find the distribution of final orbital properties for these solar systems by considering the entire collection of surviving planets and binning their orbital elements. For our first ensemble of simulations, those with $m_P = 1 m_J$, Fig. 3 shows the resulting distributions of system properties: (a) the number of surviving planets, (b) semi-major axis, (c) eccentricity, and

(d) inclination angle measured with respect to the original plane of the solar system. Figs. 4 – 6 show the same sets of distributions for the other three ensembles of simulations. Several trends are evident from these distributions, as outlined below.

The number of surviving planets (after 1 Myr) shows a reasonably wide distribution for all four ensembles. However, the case of $m_P = 1 m_J$ planets shows the widest distribution as well as the largest number of surviving planets. This result is due to two effects. First, the time scales for dynamical relaxation are longer and hence this ensemble of solar systems is dynamically less evolved. Second, the lower mass of the planets allows for larger numbers of planets to survive. To understand the importance of these two effects, we can compare the simulations with $m_P = 1 m_J$ at 1 Myr with the $m_P = 2 m_J$ simulations at 0.25 Myr (these two classes of systems should be dynamically relaxed to the same extent). The evolutionary trends shown in Figure 2 indicate that the $m_P = 1 m_J$ solar systems have, on average, 5.32 planets at the end of 1 Myr; for comparison, the $m_P = 2 m_J$ solar systems have 5.43 planets at 0.25 Myr. The uncertainty in these mean values, due to the finite sample size ($N = 100$) is about ± 0.1 planets, so that most of the difference between the two sets of simulations can be attributed to the difference in evolutionary time scales. (For further discussion of the effects of time scales, see §3.6 and Table IV for the results of 10 Myr simulations.)

For all four ensembles, the distribution of semi-major axis for the surviving planets exhibits a well-defined peak at modest values ($a \sim 10$ AU) and a long tail extending out to 150 AU (five times the original outer edge of the solar systems). As expected, the detailed shape of the distribution varies with the mass distribution of planets (compare Figs. 3, 4, 5, and 6). For all four mass choices, the distribution of eccentricity for the surviving planets spans the full range $0 \leq \epsilon \leq 1$, with a broad peak near the center of the range $\epsilon \sim 1/2$. The distribution of inclination angles (measured with respect to the starting plane of the system) shows a somewhat broad, but still well-defined peak at $i = 20 - 30$ degrees. Although the distributions of i extend up to $i = 90$ degrees, they fall off rapidly from the peak near 30 degrees.

The distributions of “final” system properties can be characterized by finding the expectation value $\langle x \rangle$ and the standard deviation σ for each variable x . These results are presented in Table II, where each entry is written in the form $\langle x \rangle \pm \sigma$ (the variables are the number \mathcal{N} of surviving planets, semi-major axis a , eccentricity ϵ , and inclination angle i). Keep in mind that the standard deviation σ represents the width of the distribution. The expectation values $\langle x \rangle$ are determined to within an uncertainty given by $\delta\langle x \rangle \approx \sigma/\sqrt{N} = \sigma/10$.

The masses of the surviving planets represent another physical variable to consider – especially for the ensemble of solar systems with randomly chosen masses. The surviving planets tend to have larger masses than the ejected ones. The expectation value and standard deviation for the mass distribution of surviving planets are also included in Table II. If the surviving planets were drawn from the same mass distribution as the starting state, the mean would be only $2.0 m_J$. The evolution from $\langle m \rangle = 2.0 m_J$ to $\langle m \rangle = 2.9 m_J$ is thus the signature of the mass segregation process

acting in these systems.

(Table II: Solar System Properties at 1 Myr)

During the course of dynamical relaxation, the loss of planets can take place through two different channels: outright ejection from the solar system or through a collision with the central star (and the subsequent accretion of the planet). The last line in Table II lists the percentage of planets that are lost through collisions with the central star for the four mass distributions. The other planets are lost through ejection events. Notice that as the distribution of planetary masses becomes wider, a smaller fraction of planets are lost through collisions with the star (a larger fraction are ejected).

Although the solar systems are not fully relaxed at the end of the 1 Myr integration interval, most of the ejections yet to take place will occur in the outer parts of the solar systems. The ensemble with $m_p = 1 m_J$ has a longer relaxation time and hence is less evolved at the 1 Myr mark. Comparison of its distributions (Fig. 3) with those of the other mass distributions (Figs. 4 – 6) show that mainly the outermost planets will be ejected in the future. This result makes sense because the outer parts of the system have a longer dynamical time and are less evolved. By comparison, the inner parts of the solar systems (say, where $a < 10$) are expected to evolve much less.

3.3. Inner Planets and their Orbital Elements

For the class of solar systems studied here, the innermost surviving planet is often in an orbit with $a \sim 1 - 2$ AU. These innermost planets are the ones that would be detected in the ongoing planet searches using radial velocity measurements. It is thus of interest to characterize the orbital properties of these inner planets and compare the results to those found in observational surveys. The orbital parameters for the innermost planets are summarized in Table III.

(Table III: Orbital Properties of the Innermost Planets)

Distributions of the orbital parameters for the inner planets are shown in Fig. 7. The upper panel shows the cumulative distribution of semi-major axis a for each of the four choices for the starting mass distribution. In all four cases, the distribution has the majority of the planets inside 5 AU – the starting inner boundary for the simulations. The differential distribution (not shown) rises toward smaller values of a and reaches a well-defined peak near $a = 1$ AU. In contrast, the distribution of eccentricity shows that ϵ is equally likely to be anywhere in the range $0 \leq \epsilon \leq 1$. For comparison, the bottom panel of Fig. 7 also shows the cumulative eccentricity distribution for observed extrasolar planets with $a \geq 0.1$ AU. The mass distribution with logarithmically spaced masses comes closest to matching the observed distribution of eccentricities, but all of the simulations produce too many planets at the highest values of ϵ . Notice also that the inclination angle

does not matter for comparison with observed single-planet systems. If only the innermost planet is detected, the plane of its orbit defines the plane of the system, independent of its initial orbital plane.

The distributions of semi-major axes a shown in Fig. 7 can be characterized as follows. For three of the four mass distributions, approximately one third of the solar systems have an inner planet with $a \leq 2$ AU; the mass distribution with m_P randomly distributed in $\log m$ shows somewhat fewer planets with such small a . For all four mass distributions, however, nearly half of the systems produce inner planets with $a \leq 3$ AU. These results show that the inward migration of giant planets (to $a \sim 1$ AU) through dynamical relaxation in crowded solar systems is easily achieved. On the other hand, this mechanism is not effective for moving planets much further inward, unless additional giant planets are present at smaller radii. The simulations show a relatively well-defined boundary at $a = 1$ AU, beyond which no planets are found.

This effective boundary at 1 AU can be understood on energetic grounds: Since all of the planets start at larger radii with $a \geq 5$ AU, migration to 1 AU results in the orbital binding energy increasing by (at least) a factor of 5. In order to conserve energy, the ejected planets (or those scattered to large a) must remove this energy from the orbit of the migrating planet. Note that the ejected planets have total energy close to zero, i.e., they carry away a relatively small amount of energy. Simple accounting shows that for one planet to move to 1 AU, the energy released is enough to disperse nearly all of the other 9 planets in the system. This argument can be made more rigorous: The Appendix presents an idealized calculation of the mass and density profile for a disk of scattering bodies that is maximally efficient at moving planets inward.

Although the solar systems are not necessarily fully relaxed as a whole, the inner portions are relatively stable. As one measure of the stability of the innermost planets, we can find the ratio of a_1/a_2 for each system, where a_1 (a_2) is the semi-major axis of the first (second) planet. For the solar systems that result in an inner planet with $a_1 \leq 2$ AU (i.e., those cases that are candidates for explaining the observed eccentric giant planets), the average value of the ratio $\langle a_2/a_1 \rangle$ is near 20. For comparison, the dynamical stability limit for a large companion with periastron p_2 interacting with a smaller planet with orbital radius a_1 is only $p_2/a_1 \approx 7$ (David et al. 2002; see also Gladman 1993). As a second measure of stability, we can consider the ratio R of the periastron of the second planet to the apastron of the innermost planet, i.e., $R = a_2(1 - \epsilon_2)/(a_1(1 + \epsilon_1))$. Fig. 8 plots the cumulative distribution of R for the four sets of simulations. For the uniform and logarithmic random mass distributions, the ratio $R \geq 2$ for the vast majority of the solar systems. For the two mass distributions with a single mass value, however, a few of the solar systems have $R < 1$ (crossing orbits) and $R \sim 1$ (unstable orbits). These solar systems will thus undergo further dynamical evolution. Nonetheless, most of the solar systems have relatively large values of R (for all four mass distributions) and are expected to be stable.

This analysis shows that dynamical relaxation is efficient at producing stable planetary orbits with semi-major axis $a \sim 1$ AU and the full range of possible eccentricity. As a result, the immediate

output of these simulations can account for a fraction of the orbits of observed extra-solar planets. Nonetheless, the distributions of orbital properties differ from those of the observed planets in two respects. The first is that the observed planets tend not to have the very highest eccentricities. However, planets with very high eccentricity tend to be the most unstable and are most likely be affected by stellar tides (if the pericenter is not too much larger than the stellar radius). As a result, they are least likely to remain in the same orbits over longer times. The other discrepancy (already mentioned) is that this mechanism – by itself – does not produce many planets with shorter periods (significantly less than one year). Keep in mind, however, that this result depends on the starting conditions, where 10 planets are assumed to populate the range $5 \text{ AU} \leq a \leq 30 \text{ AU}$.

3.4. Chaotic Dynamics

A fundamental feature of crowded planetary systems is that they are highly chaotic – in the technical sense – so that nearby trajectories in phase space diverge exponentially in time (e.g., Ruelle 1989). For the dynamical systems studied in this paper, the six phase space variables of all ten planets exhibit chaotic behavior. At a given time, the systems can be characterized by a collection of Lyapunov exponents, which represent the rate at which nearby trajectories in phase space diverge. In this subsection, we obtain a measure of these exponents λ by using a shadowing method to compute parallel trajectories for a collection of starting configurations.

If the difference between nearby trajectories grows exponentially in time, the growth rate λ is defined through the relation

$$\lambda(t) \equiv \frac{\ln[\Delta_X(t)/\Delta_{X0}]}{t}, \quad (5)$$

where Δ_X is the difference in a given phase space variable X at time t and Δ_{X0} is the difference in that variable at the beginning of the time interval. For each trial, we obtain an exponent λ for each of the 10 planets and each of the 6 phase space variables (60 values of λ). Although the exponents vary from case to case, the data show no discernible trends from planet to planet or from variable to variable. By averaging the 60 exponents for a given trial, we obtain a well-defined mean value $\langle \lambda \rangle$. Through repeated trials, we estimate the mean exponent for a longer time span. In practice, we sample the exponential divergence every 1000 years, and integrate for a total of 30,000 years.

For Jupiter mass planets, $\langle \lambda \rangle \approx 0.045 \text{ yr}^{-1}$, which implies the corresponding time scale $\tau_\lambda = \langle \lambda \rangle^{-1} \approx 22$ years. These planetary systems are thus highly chaotic. With a growth time of only about 22 years, small perturbations (e.g., with starting amplitude $\sim 10^{-6}$) will become nonlinear in only 300 years. Since we are interested in dynamical results on much longer time intervals, the results of any simulation must be presented and interpreted statistically.

3.5. Scattering into Resonant Configurations

Within the collection of 11-body simulations that were performed, a common outcome consists of two or three planets in a configuration that exhibits orbital stability over time scales $\tau > 10^6$ yr. We checked all such systems for low-order mean-motion commensurabilities among the remaining planets, and found that $\sim 10\%$ of the configurations are *near* resonance after 1 Myr (roughly equally distributed among the 2:1, 3:2, and 1:1 resonances). In every case examined, the libration widths of the resonant arguments are rather large; this result is expected because the simulations lack a dissipative mechanism (such as interactions with a remnant gaseous disk). Over longer spans of time, these systems can evolve further and many will leave resonance, due to the large libration widths and the possible loss of additional planets from the system. But resonant configurations will survive in some cases and hence multiple-planet scattering might account for systems such as HD 82943 (Udry et al. 2001) in which a pair of planets ($P_b = 444.6\text{d}$, $P_c = 221.6\text{d}$) have large eccentricities ($\epsilon_b = 0.41$, $\epsilon_c = 0.54$) and experience large librations of the 2:1 resonant angles. A more extensive treatment should be done to calculate the odds of systems attaining various resonant configurations.

Several percent of the simulations yield systems in which two planets participate in a 1:1 co-orbital resonance. An example is shown in Fig. 9. The panel at the lower left shows the time history of the system during the final million years of the simulation. The figure also shows the quantities $a(1 - \epsilon)$, and $a(1 + \epsilon)$ for each of three surviving planets in the configuration. The outer two planets are participating in a co-orbital “eccentric” resonance of the type recently described by Laughlin & Chambers (2002). The planets exchange energy and angular momentum over a secular time scale of roughly 50,000 years, and represent a stable (albeit complex) resonant configuration. Sample trajectories of the planets are plotted in the upper two frames of the figure, while the radial velocity curve of the star (over 15 orbital periods) is shown at the lower right. In this radial velocity curve, the stellar reflex velocity due to the inner planet has been removed. The plotted residual thus represents the influence of the dynamically interacting 1:1 resonant pair. This residual radial velocity curve maintains periodicity, but it deviates significantly from purely Keplerian motion, and shows complicated variations even on timescales that are considerably shorter than the $\sim 5 \times 10^4$ year period for secular eccentricity exchange.

3.6. Additional Numerical Experiments

The primary ensembles of simulations (described above) provide a basic understanding of the dynamics of these crowded planetary systems over the first 1 Myr. Nonetheless, the parameter space available for such systems is extensive and several issues remain. One important issue is to examine the longer term evolution of these systems. Another issue is that the innermost planet in the simulations can easily migrate inward to $a \sim 1$ AU (for starting configurations with $a \geq 5$ AU), but typically no further. Since observed eccentric giant planets can reside at smaller values of a , it

is useful to explore alternate mass distributions to see if further inward migration can be attained. In this subsection, we address these issues through additional sets of numerical simulations.

To study the longer-term evolution of these systems, we have carried out additional simulations using a longer time interval – 10 million years. We have performed these integrations for two of the mass distributions: case [C], where the masses are selected randomly (but uniformly) from the range $0 \leq m_P \leq 4m_J$, and case [D], where the masses are chosen randomly in $\log m$ from the range $-1 \leq \log_{10}[m_P/m_J] \leq 1$. In all cases, the simulations are started with 10 planets in circular orbits that are logarithmically spaced over the radial range $5 \text{ AU} \leq r \leq 30 \text{ AU}$. For both mass distributions, we have performed $N = 50$ simulations.

The resulting solar systems (at an evolutionary time of 10 Myr) have a distribution of properties, as summarized in Table IV. The upper half of the table shows the mean values and widths of the distributions for the number of surviving planets \mathcal{N} , the semi-major axis a , the eccentricity ϵ , the inclination angle i , and the planet mass m_P (these data should be compared with those in Table II, for the corresponding systems at 1 Myr). The lower portion of the table gives the fraction of surviving planets with $a < 2 \text{ AU}$, as well as the values of semi-major axis a_1 , eccentricity ϵ_1 , and mass m_1 for those inner planets (with $a < 2$). The ratio of the semi-major axis of the second planet to that of the inner planet is also listed (compare with Table III).

(Table IV: Solar System Properties at 10 Myr)

These longer term simulations show how much dynamical evolution takes place in these solar systems between 1 Myr and 10 Myr. The results of the 10 Myr simulations are much like the shorter ones. The mean number of surviving planets decreases from $\mathcal{N} \sim 2.5$ to $\mathcal{N} \sim 2$ over this time interval. The mean eccentricity also decreases and suggests that the high eccentricity planets are the ones lost from the system. The mean mass of the surviving planets increases, as expected if the smaller planets are more likely to be ejected.

We also performed another set of simulations that start with one large planet and 19 smaller bodies. The large planet has the mass of Jupiter and begins with a semi-major axis $a_0 = 5 \text{ AU}$ (much like the orbit of Jupiter in our solar system). The 19 smaller bodies have randomly chosen masses that are uniformly distributed over the range $0 \leq m \leq 0.5m_J$. These smaller bodies begin in circular orbits with radii evenly distributed in $\ln r$ over the range $3 \text{ AU} \leq r \leq 30 \text{ AU}$. This wider range of starting orbital radii was used so that the region inside the ‘Jupiter’ would be populated by smaller bodies. In this case, we have carried out $N = 100$ simulations to obtain a good statistical description of the outcomes.

The results show that the large planet migrates inward to become the innermost planet in 75 percent of the trials. For those cases in which the large planet becomes the innermost planet, the relevant orbital parameters exhibit distributions characterized by $\langle a \rangle = 2.08 \text{ AU} \pm 1.28 \text{ AU}$, and $\langle \epsilon \rangle = 0.36 \pm 0.20$. This starting configuration is efficient at transporting the large planet inward. Half of the simulations end with the large planet at $a < 2 \text{ AU}$, and 20 percent of the trials result

in $a < 1.5$ AU. However, only one trial places the large planet with semi-major axis $a < 1$ AU. This effective boundary at about 1 AU can be understood on energetic grounds (see §3.3 and the Appendix).

4. PLANET INTERACTIONS WITH BACKGROUND DISK TORQUES

The dynamical relaxation calculations of the previous section illustrate the difficulty in moving planets inward past 1 AU (for planets starting with $a \geq 5$ AU). Although a wide range of final system properties can be realized through dynamical relaxation of 10 planet systems, the observed extra-solar planets often reside in orbits with shorter periods (smaller semi-major axes a). One way to achieve shorter periods is through tidal interactions of the planet with the gaseous disk that gave it birth (e.g., Goldreich and Tremaine 1980; Lin, Bodenheimer, and Richardson 1996; Bryden et al. 2000), although this mechanism does not generally produce high eccentricities. Another way to achieve shorter periods is through gravitational scattering interactions with a disk of planetesimals (Murray et al. 1998). This latter mechanism requires a great deal of mass in solid materials inside the orbit of the giant planet (see Murray et al. 1998; see also the Appendix for a limiting case). In this section, we explore the implications of combining dynamical relaxation of two planets with the inward forcing driven by tidal interactions with a background nebular disk (see also Kley 2000; Murray, Paskowitz, and Holman 2002).

Specifically, we set up the following type of numerical experiments: Two planets are placed on widely spaced orbits. The inner planet is started with an orbital period of 1900 days, corresponding to a semi-major axis of about 3 AU (a stellar mass of $M_* = 1.0 M_\odot$ is used throughout). The initial period of the outer planet is larger by a factor of $\pi^{2^{1/4}} \approx 3.736 \dots$. This period ratio is an irrational number (more precisely, a 14 digit approximation to an irrational number), so the planets are not started in resonance. As the outer planet loses orbital energy and angular momentum through tidal torques, however, it moves inward and the two planets can eventually be caught in resonances (see, e.g., Lee and Peale 2002), typically the 3:1 resonance in this case. The initial eccentricities of both planets are drawn from a random distribution in the range $0 < \epsilon < 0.05$. The planet masses are drawn independently from a random distribution in the range $0 < m_P < 5m_J$. These numerical experiments are thus quite similar to those carried out by Snellgrove, Papaloizou and Nelson (2001), in their study of the GJ 876 system, and by Laughlin, Chambers & Fischer (2002) in their analysis of the 47 UMa system. Our goal here is to build on these previous studies by producing a statistical generalization of the generic migration problem with two planets and an exterior disk – a situation that we expect is quite common during the planet formation process.

The outer planet in the system is assumed to be tidally influenced by a background circumstellar disk. Instead of modeling the planet/disk interaction in detail, however, we introduce a frictional damping term into the dynamics. This damping force has the form $\mathbf{f} = -\mathbf{v}\tau_{\text{damp}}^{-1}$ and is applied to the outer planet at each time step, so the outer planet is gradually driven inward. This damping force is proportional to the velocity and defines a damping time scale τ_{damp} . In

this set of simulations, we set the damping time scale to be $\tau_{\text{damp}} = 3 \times 10^5$ yr. If disk accretion occurs through viscous diffusion and can be modeled using an ‘ α -prescription’, we can find the value of α for this choice of time scale: The disk accretion time $\tau_{\text{disk}} = \varpi^2/\nu$, where the viscosity $\nu = (2/3)\alpha v_T^2 \Omega^{-1}$ (see Shu 1992). Writing the disk scale height H in the form $H = v_T/\Omega$ (v_T is the sound speed), the accretion time becomes $\tau_{\text{disk}} = 1.5(\varpi/H)^2 \Omega^{-1} \alpha^{-1}$. If we evaluate the disk scale height H and rotation rate Ω for a temperature of $T = 70$ K at $\varpi = 7$ AU (where the outer planet begins), we find $\alpha = 7 \times 10^{-4}$ for our adopted time scale $\tau_{\text{damp}} = 0.3$ Myr. This value falls within the expected range $10^{-4} \leq \alpha \leq 10^{-2}$ (see Shu 1992). Recent estimates of this damping time scale (e.g., Tanaka, Takeuchi, and Ward 2002) are in basic agreement with the value chosen here. In this treatment, the energy dissipation time scale is assumed to be independent of the planet’s orbital eccentricity, although more complicated behavior is possible (Tanaka et al. 2002; Papaloizou and Larwood 2000).

These simulations include three additional effects. The first is the damping of the eccentricity of the outer planet by the circumstellar disk. The same angular momentum exchange between the disk and the planet that leads to orbital migration can also modify the eccentricity of the orbit (e.g., Snellgrove et al. 2001; Agnor and Ward 2002). To incorporate this effect, we allow the orbital eccentricity of the outer planet to be damped on a time scale τ_{ed} , which we consider as a free parameter. A wide range of effective values for τ_{ed} are possible (Snellgrove et al. 2001), but we adopt the range of values $\tau_{\text{ed}} = 1 - 3$ Myr for this study.

Next, we include relativistic corrections to the force equations (e.g., Landau and Lifshitz 1975; Weinberg 1972). This force correction drives the periastron of both planetary orbits to precess (in the forward direction). The effect is greater close to the star, so the inner planet experiences a greater precession, which acts to move the two planets away from a resonant condition. For planets that orbit sufficiently close to their stars, this precession can be effective in keeping the planets out of a perfect resonance. Since resonant conditions lead to more extreme growth of orbital eccentricity (which drives the system toward instability), relativistic precession acts to make planetary systems more stable. In these simulations, the planets only rarely wander close enough to the star to make this effect important, but it is nonetheless included.

Finally, for completeness, the simulations take into account energy loss due to tidal interactions between the planets and the central star. Since the planets in these simulations spend most of their time relatively far from the star, where tidal interactions are negligible, we adopt an approximate treatment of this effect. Specifically, we adopt the approximations advocated in Papaloizou and Terquem (2001), where the force exerted on the planet due to tidal interactions can be written in the form

$$\mathbf{F} = -\frac{Gm_p R_*^5}{C j r^{11}} [r^2 \mathbf{v} - (\mathbf{r} \cdot \mathbf{v}) \mathbf{r}] \frac{0.6 R_p^3}{1 + (R_p/R_*)^3}, \quad (6)$$

where R_* is the stellar radius, R_p is the distance of closest approach for a *parabolic* orbit with angular momentum j , and $C = 2\sqrt{\pi}/3$ is a dimensionless constant of order unity (see Papaloizou and Terquem 2001 for further discussion). This approximation assumes that most of the influence

occurs near the point of closest approach and that the time between encounters is long compared to the time for tidal interaction itself. This approximation is valid when the planetary orbit has high eccentricity, which is the case for the planets in these simulations (see also Press and Teukolsky 1977).

With the starting conditions described above, the numerical experiments are integrated forward in time until only one planet remains, or the integration time reaches one million years. The general evolutionary trend can be described as follows. The planets are started out of resonance, but the outer planet is forced inward by the dissipative term (which represents the action of a circumstellar disk) until the planets enter into a mean motion resonance, usually the 3:1 resonance. The two planets then migrate inwards together, near resonance, but the planetary interactions tend to increase the orbital eccentricity of both bodies. The large eccentricities drive the planet to exhibit ever-larger departures from the resonant condition. The eccentricities increase until the system becomes unstable, and a wide range of final system properties can result.

In practice, we continue the simulations until one of the planets is ejected or driven into the central star, or the two planets collide with each other. The effective radius for collisions is taken to be about $2 r_J$, where we assume that the planets have not fully contracted. After a planet is lost (via ejection, accretion, or collision), the simulation is stopped and the orbital elements of the surviving planet are calculated. However, the orbital elements of the surviving planet can continue to evolve (after a planet is lost) as long as the disk is still present. To account for this additional evolution, we assume that the inner disk has a lifetime τ_{disk} randomly drawn from a uniform distribution (with $\tau_{\text{disk}} \leq 1$ Myr). After the main integration is stopped, the orbital elements of the surviving planet are corrected for energy dissipation and eccentricity damping over the time for which the disk remains intact.

The orbital elements of the remaining planets show a distribution of properties, as summarized in Table V and Figure 10. For both choices of the eccentricity damping time scale, the numerical experiments end with about 60 percent ejections, 20 percent accretion events, and 1 percent collisions. The remaining cases reach the stopping time of 1 Myr without losing a planet. As expected, the ejected planets are more likely to be those that start as the outer planet (only about one third of the ejection events remove the inner planet). The accreted planets are almost exclusively the inner planets (in all but one case). The average time for the first planet to be ejected – for all outcomes – is about 0.5 Myr, roughly comparable to the viscous damping time of $\tau_{\text{damp}} = 0.3$ Myr. Accretion events take the longest, with an average time of 0.55 Myr; ejection events have a mean time of 0.22 Myr; collisions take place the fastest with a mean time of only 0.90 Myr. For the case of accretion or ejection events (of either planet), the distributions of semi-major axis a , eccentricity ϵ , and mass m_P are similar. The collisions result in significantly different orbital properties, with smaller eccentricity ϵ and larger mass m_P . The other general trend that emerges from this suite of simulations is that the systems that remain stable over the entire 1 Myr integration time are those with the smallest planets, with a mean mass of only $1.5 m_J$ (compared to a mean mass $m_P = 2.8 m_J$ for the whole ensemble).

(Table V: Surviving Planet Properties)

The distributions of semi-major axis and eccentricity for the surviving planets are shown in Fig. 10, which includes results for both choices of eccentricity damping time scale ($\tau_{\text{ed}} = 1$ Myr and 3 Myr). The distributions are shown both at the time when the first planet is ejected and after additional orbital evolution has taken place. This migration mechanism naturally populates the inner region of the solar systems, i.e., the range of semi-major axes $0.1 \text{ AU} \leq a \leq 1 \text{ AU}$ where dynamical relaxation (§3) is ineffective (for planets that start with $a > 5 \text{ AU}$). The distribution of semi-major axes is roughly consistent with that of the observed population of extra-solar planets. However, the simulations tend to produce too many planets with highly eccentric orbits compared to the observed sample (see the bottom panel of Fig. 10).

Another way to compare the theoretical simulations with the observed sample of extrasolar planets is through the $a - \epsilon$ plane. Fig. 11 shows this plane for the observed planets and the two choices of eccentricity damping time scale using in the numerical simulations. Although the separate distributions of a and ϵ show reasonable agreement between the theory and the observed sample, the two-dimensional distributions (in $a - \epsilon$ space) provide a stronger test. Fig. 11 shows that the observed planet population contains more orbits with both small a and small ϵ than the theoretical model (the lower left region of Fig. 11), or, equivalently, the theory produces too many orbits with high eccentricity. This trend can be quantified using a two-dimensional Kolmogorov-Smirnov (K-S) test on two samples. The K-S test provides the probability that the two samples were drawn from the same underlying population. In this case, the probability is rather low, less than one percent, and hence the two samples are indeed different. Notice that this discrepancy could be relieved by tidal circularization that takes place over time spans much longer than the 1 Myr time scale of these simulations; this mechanism acts to decrease the eccentricity of the planetary orbits.

5. SUMMARY AND DISCUSSION

This paper has explored the dynamical relaxation of giant planet systems in their early phases of evolution. By integrating a large number of equivalent realizations (e.g., $N = 100$) for each set of starting conditions, we obtain the distributions of the final system properties. The motivation for this work is both to understand the dynamics of these crowded planetary systems and to determine whether or not dynamical evolution can produce planetary orbits like those observed in the current sample of extra-solar planets.

The first dynamical result is a determination of the decay time for each class of solar system. In this context, the decay time is the time required for a solar system to either eject its first planet or accrete a planet onto the central star. Any given sample of solar systems has a well-defined half-life – the time over which half of the sample will decay (see Fig. 1 and Table I). Over longer spans of time, the solar systems continue to evolve by spreading out, ejecting planets, and accreting planets. The evolution of these systems can be described by a simple function (see Eq. [4] and Fig.

2). A related time scale is time required for a given solar system to lose half of its initial population of planets. For the ensembles studied here, this evolution time is about 12 times longer than the corresponding half-life (Table I).

All of the solar systems studied here are highly chaotic in the technical sense. To quantify this behavior, we have calculated characteristic exponents for the orbital parameters in these systems. The corresponding Lyapunov times – roughly the e-folding time for small departures between equivalent physical systems to grow – is relatively short, typically a few decades (10s of years). Putting all of the timing results together, we obtain the following ordering of time scales

$$\tau_{\text{orbit}} \ll \tau_{\text{chaos}} \ll \tau_{\text{decay}} \ll \tau_{\text{evolve}} \ll \tau_{\text{lifetime}}, \quad (7)$$

where τ_{lifetime} is the total expected lifetime of the systems (typically billions of years).

The main astronomical motivation for this work is to account for the observed extra-solar planets in highly eccentric orbits. For crowded planetary systems initially populated in the radial range $5 \text{ AU} \leq a \leq 30 \text{ AU}$, dynamical relaxation naturally produces eccentric orbits with semi-major axis $a \sim 1 \text{ AU}$. Such orbits occur readily; for example, one third of the systems successfully place planets in orbits with $a < 2 \text{ AU}$ (see Table III and Fig. 7). Although successful in producing eccentric orbits with $a \approx 1 \text{ AU}$, dynamical relaxation, acting in isolation, does not generally drive planets to migrate further inwards. The basic reason for this difficulty is that these giant planet systems do not have scattering bodies at small radii to remove further energy from the system.

The Appendix quantifies this difficulty and defines a benchmark disk model which has the minimum mass necessary to cause planetary migration through scattering events (subject to the idealizations of the calculation). To move a planet of mass m_P from a starting semi-major axis a_0 inward to a_f , the required mass is $M_{MES} = m_P \ln[a_0/a_f]$, and it must be located within the annulus $a_f \leq r \leq a_0$ (provided that the mass moves on orbits of low eccentricity). For a giant planet to migrate inward beyond the effective boundary at $\sim 1 \text{ AU}$ found in the simulations, the disk must contain at least a planetary mass worth of scattering bodies close to the star ($a < 1 \text{ AU}$). Additional migration by giant planet scattering is thus problematic because giant planets do not readily form (presumably) in the inner solar system (hence the need for migration). But additional inward migration by planetesimals – another leading candidate – is also problematic: Although the inner solar system naturally produces such entities, they are made of heavy elements. To move a Jupiter-mass planet from $a = 1 \text{ AU}$ to $a = 1/3 \text{ AU}$, for example, the disk must contain about 370 Earth masses of rocky material *within 1 AU of the star*.

This work also demonstrates that dynamical instability in crowded planetary systems can result in a pair of surviving planets which are participating in large-amplitude librations around low-order mean-motion resonances. In particular, multiple-planet scattering can lead to pairs of planets in unusual co-orbital resonances, including the 1:1 eccentric resonance shown in Fig. 9. Short-term dynamical interactions of such a configuration would lead to a readily detectable radial velocity signature.

As an alternate migration scenario, we have explored the possibility of multiple giant planets being driven inward through the action of tidal torques in a circumstellar disk. In this case, the outer planet interacts with the disk and has energy and angular momentum drained away from its orbit. As the outer planet migrates inward, it eventually becomes close enough to the interior planet to drive eccentricity growth and increasingly violent interactions. Such systems are not stable in the long term and adjust themselves to stability by ejecting a planet, accreting a planet onto the central star, or by having the two planets collide. The surviving planet is left on an eccentric orbit of varying semi-major axis, i.e., $0.1 \leq a \leq 3$ AU (see Fig. 10 and Table V).

In addition to the specific results described above, the results of this investigation illustrate a more general aspect of solar system formation and dynamics. Although the planet formation process can proceed through many different channels – or at least many scenarios for planet formation remain viable – all of them lead to dynamical systems that are highly chaotic (see Eq. [7]). Even the most sedate end result – a well-ordered solar system like our own – displays chaotic behavior over sufficiently long spans of time. In the face of such chaos, the results of the planet formation process must be described in terms of a full *distribution* of results. Given the enormous variation possible, and the extreme sensitivity to initial conditions, it does not make sense to talk about a single outcome of any given dynamical experiment; and this result applies to both theoretical calculations of planet formation and the experiments done by planet-forming systems in our galaxy.

Acknowledgements

During the course of this work, we have benefited from discussions with Gus Evrard and Elisa Quintana. We would also like to thank the referees (Eric Ford and a second anonymous referee) for many useful suggestions that improved this paper. This work was supported in part by NASA through the Origins of the Solar System Program and by the University of Michigan through the Michigan Center for Theoretical Physics.

APPENDIX: THE MAXIMALLY EFFICIENT SCATTERING DISK

In this Appendix, we derive a limiting form for the surface density distribution and disk mass necessary to drive planetary migration through scattering interactions. For the sake of definiteness, we consider a migrating giant planet of mass m_P and initial semi-major axis a_0 . The starting energy of its orbit is thus $E_0 = -GM_*m_P/2a_0$. In order to migrate inward, the planet must have energy removed from its orbit so that it falls deeper into the gravitational potential well of its parental star. In this idealized calculation, we assume that the requisite loss of energy takes place through scattering interactions, where the scattering bodies have mass μ and move on orbits of low eccentricity. The scattering bodies could be either planetessimals (small μ) or other planets (larger μ). In this first approximation, each scattering interaction takes place at radius r and removes energy $\Delta E = -GM_*\mu/2r$ from the orbit of the planet. This energy increment is that required for the scattering body to become unbound (at zero energy) from a circular orbit at radius r .

After one scattering interaction, the semi-major axis of the migrating giant planet becomes

$$a_1 = a_0(1 + \mu/m_P)^{-1}, \quad (\text{A1})$$

where we have assumed that the planet moves as far inward as possible without violating conservation of energy. The disk is assumed to be maximally efficient in the sense that for every new orbit the giant planet obtains, a new scattering body will be present to scatter and remove further energy from the planet's orbit. If the planet moves as far inward as possible, each scattering will decrease the semi-major axis by the same factor. After n scattering interactions, the new orbit attain a semi-major axis a_n given by

$$a_n = a_0(1 + \mu/m_P)^{-n}. \quad (\text{A2})$$

Let $f_n \equiv a_0/a_n$ be the factor by which the semi-major axis decreases after n steps. The total mass M_S in scattering bodies is related to the mass of the bodies via $M_S = n\mu$. The factor f_n can then be written in the form

$$f_n = \left(1 + \frac{M_S/m_P}{n}\right)^n. \quad (\text{A3})$$

For a fixed mass M_S in scattering bodies, the factor f_n increases (slowly) with increasing n , so the maximum migration factor can be defined by taking the limit $n \rightarrow \infty$. The maximum factor is thus given by

$$\lim_{n \rightarrow \infty} f_n = e^{M_S/m_P}. \quad (\text{A4})$$

In other words, the minimum mass M_{MES} in scattering bodies required to move a planet from a_0 to a_f can be written in the form

$$M_{MES} = m_P \ln[a_0/a_f]. \quad (\text{A5})$$

For typical migration patterns, $a_0 \approx 5$ AU and $a_f \approx 0.1$ AU, so $M_S > \ln[50]m_P$. If $m_P = m_J$, for example, then the mass M_S of scattering bodies must exceed about 4 Jupiter masses or 1200 times the mass of Earth.

This result suggests that migration over large distances via scattering processes is problematic for any likely mass of the scattering bodies. If the scattering entities are giant planets, then the mass requirements are reasonable, but the scattering bodies – which are giant planets themselves – must already reside at inner locations in the solar system. The scattering calculations of this paper show that giant planet systems will rarely scatter multiple planets to small a so that they can scatter off of each other to even smaller a . Migration factors of $f = 5$ are readily obtained, whereas factors of $f = 50$ are (almost) never realized in the numerical experiments.

On the other hand, if the scattering bodies are planetessimals – which are made of heavy elements – then location is no longer a problem, but the amount of mass required is excessive. For example, our solar system contains a total of only 100 Earth masses worth of rocky material, a factor of 13 too small to attain a migration factor of $f = 50$. If migration is limited to metal rich systems, and if early solar systems have more mass than the minimum mass solar nebula, then the total inventory of planetessimals could approach the necessary minimum value. But even in such a favorable case, most of the disk mass (and hence the rocky material) is expected to lie in the outer solar system, whereas migration through scattering requires it to reside in the inner solar system.

The maximally efficient scattering disk, as defined here, displays a particular distribution of surface density. In discrete form, the surface density can be written

$$\sigma(r) = \sum_{k=0}^{n_f-1} \frac{\mu}{2\pi r} \delta(r - a_k), \quad (\text{A6})$$

where $\delta(x)$ is the Dirac delta function and the positions a_k are determined through Eq. [A2]. Taking the limit $n \rightarrow \infty$, $\mu \rightarrow 0$, with $n\mu \rightarrow \text{constant}$, we obtain a surface density profile of the form

$$\sigma_{MES}(r) = \frac{m_P}{2\pi r^2}. \quad (\text{A7})$$

As a consistency check, notice that if we integrate the surface density profile [A7] over an annulus of outer radius r_0 and inner radius r_f , the mass enclosed is given by $\Delta M = m_P \ln[r_0/r_f]$, in agreement with Eq. [A5].

REFERENCES

- Adams, F. C., and G. Laughlin 2001. Constraints on the birth aggregate of the solar system. *Icarus* **150**, 151 – 162.
- Adams, F. C., S. P. Ruden, and F. H. Shu 1989. Eccentric gravitational instabilities in nearly Keplerian disks. *Astrophys. J.* **347**, 959 – 976.
- Agnor, C. B., and W. R. Ward 2002. Damping of terrestrial-planet eccentricities by density-wave interactions with a remnant gas disk. *Astrophys. J.* **567**, 579 – 586.
- Binney, J., and S. Tremaine 1987. *Galactic Dynamics*. (Princeton: Princeton Univ. Press).
- Boss, A. P. 2000. Possible rapid gas giant formation in the Solar nebula and other protoplanetary disks. *Astrophys. J.* **536**, L101 – 104.
- Bryden, J., M. Rózyczka, D.N.C. Lin, and P. Bodenheimer 2000. On the interaction between protoplanets and protostellar disks. *Astrophys. J.* **540**, 1091 – 1101.
- Cameron, A.G.W. 1978. Physics of the primitive solar accretion disk. *Moon and Planets* **18**, 5 – 40.
- Chambers, J. E. 1999. A hybrid symplectic integrator that permits close encounters between massive bodies. *Mon. Not. R. Astron. Soc.* **304**, 793 – 799.
- Chambers, J. E., G. W. Wetherill, and A. P. Boss 1996. The stability of multi-planet systems. *Icarus* **119**, 261 – 268.
- David, E.-M., E. V. Quintana, M. Fatuzzo, and F. C. Adams, 2002. Dynamical Stability of Earth-like Planetary Orbits in Binary Systems. submitted to *Publ. Astron. Soc. Pacific*
- Duncan, M. J., and T. Quinn 1993. The long-term dynamical evolution of our solar system. *Ann. Rev. Astron. Astrophys.* **31**, 265 – 295.
- Ford, E. B., M. Havlickova, and F. A. Rasio 2001. Dynamical instabilities in extrasolar planetary systems containing two planets. *Icarus* **150**, 303 – 313.
- Ford, E. B., F. A. Rasio, and K. Yu 2002. Dynamical instabilities in extrasolar planetary systems. astro-ph/0210275
- Gladman, B. 1993. Dynamics of systems of two close planets. *Icarus* **106**, 247 – 258.
- Goldreich, P., and S. Tremaine 1980. Disk-satellite interactions. *Astrophys. J.* **241**, 425 – 441.
- Gonzalez, G. 1997. The stellar metallicity-giant planet connection. *Mon. Not. R. Astron. Soc.* **285**, 403 – 412.

- Hatzes, A. P., et al. 2000. Evidence for a long period planet orbiting Epsilon Eridani. *Astrophys. J.* **529**, L145 – 148.
- Katz, J. I. 1997. Single close encounters do not make eccentric planetary orbits. *Astrophys. J.* **484**, 862 – 865.
- Kley, W. 2000. On the migration of a system of protoplanets. *Mon. Not. R. Astron. Soc.* **313**, L47 – L51.
- Landau, L. D., and E. M. Lifshitz 1975. The classical theory of fields. (New York: Pergamon Press).
- Laskar, J. 1990. The chaotic motion of the solar system – A numerical estimate of the size of the chaotic zones. *Icarus* **88**, 266 – 291.
- Laughlin, G. 2000. Mining the metal-rich stars for planets. *Astrophys. J.* **545**, 1064 – 1073.
- Laughlin, G., and F. C. Adams 2000. The frozen Earth: Binary scattering events and the fate of the solar system. *Icarus* **145**, 614 – 627.
- Laughlin, G., and J. E. Chambers 2002. Extrasolar trojans: The viability and detectability of planets in the 1:1 resonance. *Astron. J.* **124**, 592 – 600.
- Laughlin, G., J. E. Chambers, and D. Fischer 2002. A dynamical analysis of the 47 Ursae Majoris planetary system. *Astrophys. J.* **579**, 455 – 467.
- Lee, M. H., and S. J. Peale 2002. Dynamics and the origin of the 2:1 orbital resonances of the GJ876 planets. *Astrophys. J.* **567**, 596 – 609.
- Levison, H. F., J. J. Lissauer, and M. J. Duncan 1998. Modeling the diversity of outer planetary systems. *Astron. J.* **116**, 1998 – 2014.
- Lin, D.N.C., P. Bodenheimer, and D. C. Richardson 1996. Orbital migration of the planetary companion of 51 Pegasi to its present location. *Nature* **380**, 606 – 607.
- Lin, D.N.C., and S. Ida 1997. On the origin of massive eccentric planets. *Astrophys. J.* **477**, 781 – 791.
- Lin, D.N.C., and J.C.B. Papaloizou 1993. On the tidal interaction between protostellar disks and companions. in *Protostars and Planets III*, eds. E. H. Levy and J. I. Lunine. (Tucson: Univ. Arizona Press), pp. 749 – 836.
- Lissauer, J. J. 1987. Timescales for planetary accretion and the structure of the protoplanetary disk. *Icarus* **69**, 249 – 265.
- Lissauer, J. J. 1993. Planet formation. *Ann. Rev. Astron. Astrophys.* **31**, 129 – 174.
- Marcy, G. W. and R. P. Butler 1996. A planetary companion to 70 Virginis. *Astrophys. J.* **464**, L147 – 150.

- Marcy, G. W. and R. P. Butler 1998. Detection of extrasolar giant planets. *Ann. Rev. Astron. Astrophys.* **36**, 57 – 97.
- Marcy, G. W., and R. P. Butler 2000. Planets orbiting other suns. *Publ. Astron. Soc. Pacific* **112**, 137 – 140.
- Marzai, F., and Weidenschilling, S. J. 2002. Eccentric extrasolar planets: The jumping Jupiter model. *Icarus* **156**, 570 – 579.
- Mayor, M., and D. Queloz 1995. A Jupiter-mass companion to a solar-type star. *Nature* **378**, 355 – 359.
- Murray, N., B. Hansen, M. Holman, and S. Tremaine 1998. Migrating Planets. *Science* **279**, 69 – 71.
- Murray, N., M. Paskowitz, and M. Holman 2002. Eccentricity evolution of migrating planets. *Astrophys. J.* **565**, 608 – 620.
- Nelson, R. P., J.C.B. Papaloizou, F. Masset, and W. Kley. 2000. The migration and growth of protoplanets in protostellar discs. *Mon. Not. R. Astron. Soc.* **318**, 18 – 36.
- Papaloizou, J.C.B., and C. Terquem 2001. Dynamical relaxation and massive extrasolar planets. *Mon. Not. R. Astron. Soc.* **325**, 221 – 230.
- Papaloizou, J.C.B., and J. D. Larwood, 2000. On the orbital evolution and growth of protoplanets embedded in a gaseous disc. *Mon. Not. R. Astron. Soc.* **315**, 823 – 833.
- Perryman, M.A.C. 2000. Extra-solar planets. *Inst. Phys. Rep. Progress Phys.* **63**, 1209 – 1272.
- Press, W. B., and S. A. Teukolsky 1977. On the formation of close binaries by two-body tidal capture. *Astrophys. J.* **213**, 183 – 192.
- Rasio, F. A., and E. B. Ford 1996. Dynamical instabilities and the formation of extrasolar planetary systems. *Science* **274**, 954 – 956.
- Ruelle, D. 1989. *Chaotic Evolution and Strange Attractors*. (Cambridge: Cambridge Univ. Press).
- Shu, F. H. 1992. *Gas Dynamics*. (Mill Valley: Univ. Science Books).
- Snellgrove, M. D., J.C.B. Papaloizou, and R. P. Nelson 2001. On disc driven inward migration of resonantly coupled planets with application to the system around GJ876. *Astron. Astrophys.* **374**, 1092 – 1099.
- Tanaka, H., T. Takeuchi, and W. R. Ward 2002. Three-dimensional interaction between a planet and an isothermal gaseous disk: I. Corotation and Lindblad torques and planet migration. *Astrophys. J.* **565**, 1257 – 1274.

- Terquem, C., and J.C.B. Papaloizou 2002. Dynamical relaxation and the orbits of low-mass extrasolar planets. *Mon. Not. R. Astron. Soc.* **332**, L39 – L43.
- Trilling, D. E., W. Benz, T. Guillot, J. I. Lunine, W. B. Hubbard, and A. Burrows 1998. Orbital evolution and migration of giant planets: Modeling extrasolar planets. *Astrophys. J.* **500**, 902 – 914.
- Udry, S., M. Mayor, D. Naef, F. Pepe, D. Queloz, and N. C. Santos 2001. A Planetary system around HD 82943. <http://obswww.unige.ch/~udry/planet/hd82943syst.html>
- Weidenschilling, S. J. and F. Marzai 1996. Gravitational scattering as a possible origin for giant planets at small stellar distances. *Nature* **384**, 619 – 620.
- Weinberg, S. 1972. *Gravitation and cosmology*. (New York: Wiley).

Table I: Characteristic Time Scales

variable / sample	$m_P = 1 m_J$	$m_P = 2 m_J$	random m_P	log-random
τ_{decay} (Myr)	0.125	0.0345	0.0185	0.00721
$\tau_{1/2}$ (Myr)	0.0866	0.0239	0.0128	0.0050
τ_{evolve} (Myr)	1.14	0.309	0.157	0.0569
α	0.932	0.596	0.440	0.304
γ (Myr) ⁻¹	0.981	6.89	22.6	143

Table II: Solar System Properties at 1 Myr

variable / sample	$m_P = 1 m_J$	$m_P = 2 m_J$	random m_P	log-random
\mathcal{N}	5.2 ± 1.2	2.9 ± 0.79	2.5 ± 0.83	2.3 ± 0.82
a (AU)	49 ± 38	44 ± 43	33 ± 37	29 ± 33
ϵ	0.53 ± 0.24	0.52 ± 0.22	0.42 ± 0.23	0.41 ± 0.20
i (degrees)	36 ± 24	34 ± 23	30 ± 21	21 ± 20
m_P (m_J)	1 ± 0	2 ± 0	2.9 ± 0.86	4.7 ± 2.9
accretion events (%)	23	15	11	5.5

Table III: Orbital Properties of the Inner Planets at 1 Myr

variable / sample	$m_P = 1 m_J$	$m_P = 2 m_J$	random m_P	log-random
$\mathcal{F}(a < 2\text{AU})$	0.37	0.29	0.33	0.09
a (AU)	1.4 ± 0.28	1.3 ± 0.28	1.6 ± 0.24	1.6 ± 0.37
ϵ	0.65 ± 0.16	0.56 ± 0.22	0.48 ± 0.21	0.61 ± 0.20
$a(1 - \epsilon)$ (AU)	0.47 ± 0.23	0.59 ± 0.30	0.83 ± 0.33	0.60 ± 0.33
$R = a_2/a_1$	15 ± 7.5	20 ± 14	21 ± 18	15 ± 9.7
m_P (m_J)	1 ± 0	2 ± 0	3.0 ± 0.52	4.3 ± 2.4

Table IV: Solar System Properties at 10 Myr

variable / sample	random m_P	log-random
\mathcal{N}	1.9 ± 0.54	2.0 ± 0.58
a (AU)	32 ± 43	24 ± 29
ϵ	0.49 ± 0.22	0.37 ± 0.21
i (degrees)	23 ± 19	18 ± 16
m_P (m_J)	3.0 ± 0.70	5.0 ± 2.6
$\mathcal{F}(a < 2\text{AU})$	0.36	0.060
a_1 (AU)	1.6 ± 0.27	1.4 ± 0.38
ϵ_1	0.58 ± 0.20	0.66 ± 0.07
m_1 (m_J)	3.1 ± 0.50	3.3 ± 0.43
$R = a_2/a_1$	25 ± 24	11 ± 7.8

**Table V: Surviving Planet Properties:
Two planets systems tidally driven by a disk (350 Trials)**

variable/sample	$\tau_{\text{ed}} = 1 \text{ Myr}$	$\tau_{\text{ed}} = 3 \text{ Myr}$
a (AU)	0.82 ± 1.25	0.91 ± 0.95
ϵ	0.45 ± 0.27	0.53 ± 0.29
m_P (m_J)	2.9 ± 1.4	2.7 ± 1.4
τ_{eject} (Myr)	0.49 ± 0.39	0.53 ± 0.40
Accretion fraction (%)	20	19
Ejection fraction (%)	62	56
Collision fraction (%)	0.5	1.2

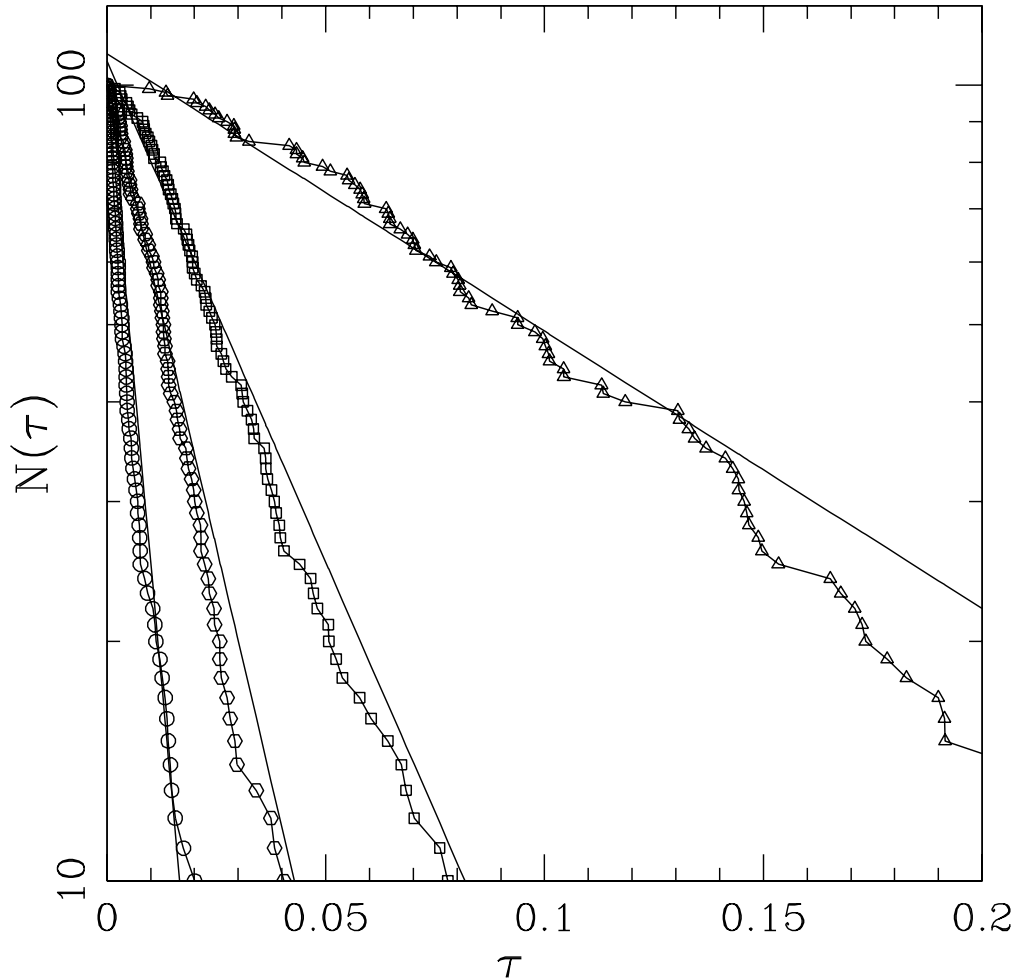


Fig. 1.— Determination of the decay time for crowded solar systems. For an ensemble of 100 numerical simulations, each curve depicts the number $N(\tau)$ of solar systems that have not decayed by ejecting or accreting a planet. The functions $N(\tau)$ are plotted versus time (in millions of years). The triangles show the results of simulations using planets with $m_P = 1 m_J$; the squares show the results for planets with $m_P = 2 m_J$; the hexagons show the results for planets with randomly chosen masses in the range $0 \leq m_P \leq 4 M_J$; the circles show the results for a planet mass distribution chosen uniformly in $\log m$ within the range $-1 \leq \log_{10}[m_P/m_J] \leq 1$. The solid lines are weighted fits to the numerical results (see text) and the slope of the lines determine the decay time (see Table I).

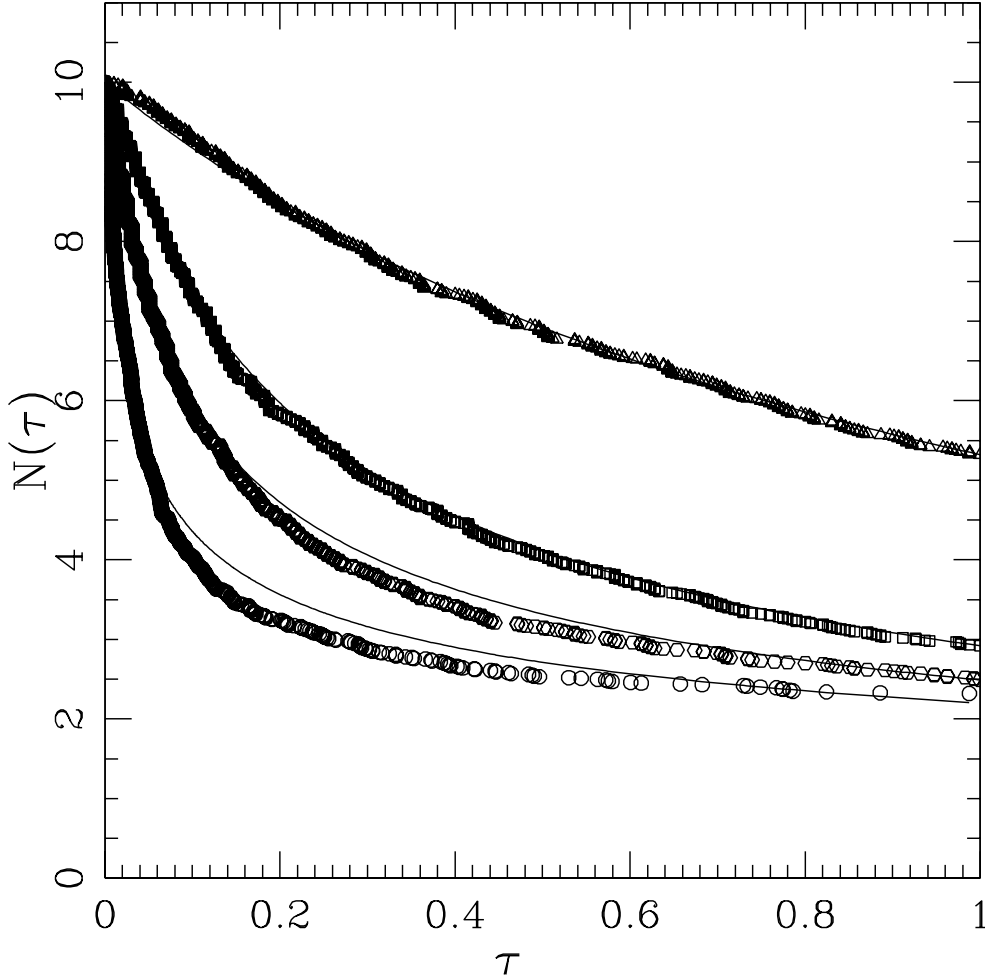


Fig. 2.— Determination of the evolutionary behavior for crowded solar systems. For each starting mass function, the entire ensemble of $N = 100$ simulations collectively determines the typical behavior for the number of surviving planets as a function of time (in millions of years). The triangles show the results for simulations using planets with $m_P = 1 m_J$; the squares show the results for planets with $m_P = 2 m_J$; the hexagons show the results for planets with randomly chosen masses in the range $0 \leq m_P \leq 4 M_J$; the circles show the results for planets with masses chosen uniformly in $\log m$ in the range $-1 \leq \log_{10}[m_P/m_J] \leq 1$. The solid curves are fitted functions of the form given by Eq. [4] (see text).

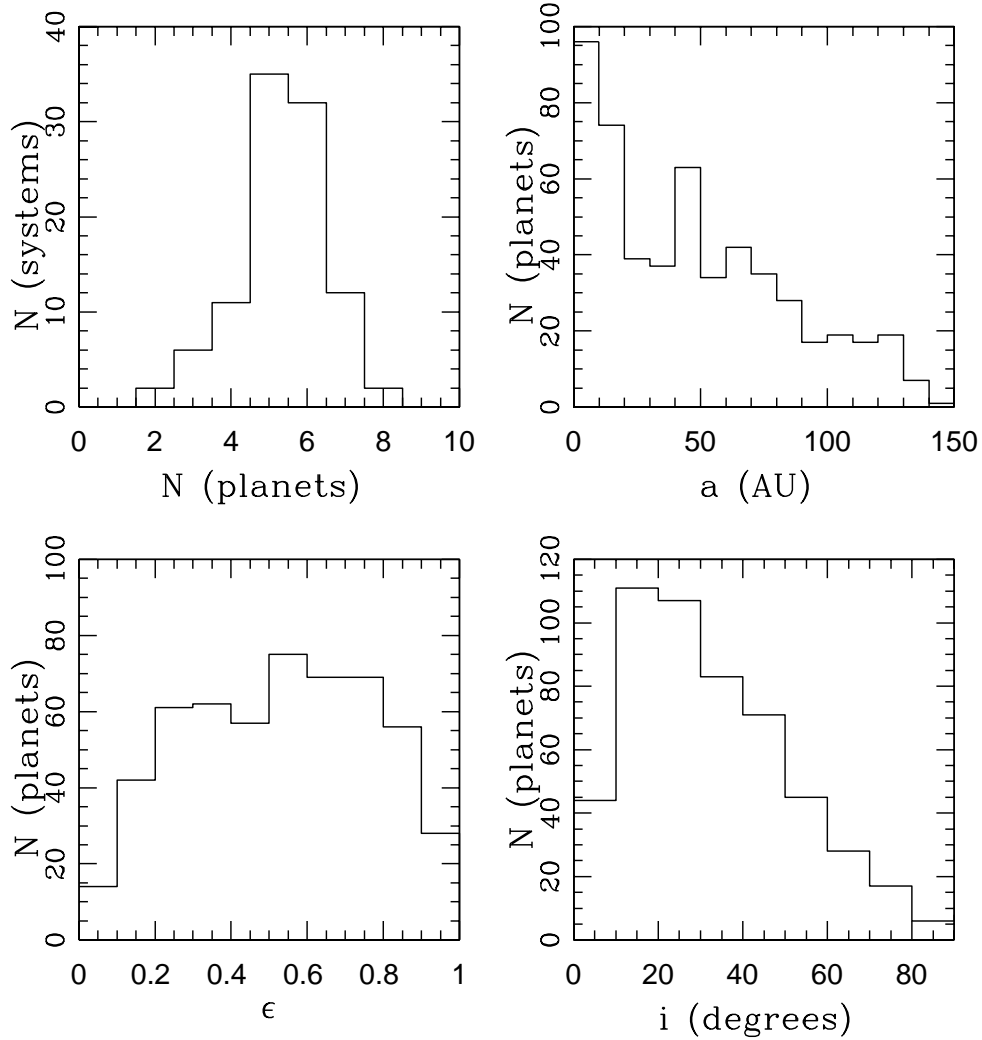


Fig. 3.— Characterization of solar system properties after 1 Myr of dynamical evolution – for the case of planets with $m_P = 1 m_J$. All of the remaining planets in the ensemble of $N = 100$ solar systems are folded together in these histograms. (a) Distribution of number of remaining planets. (b) Distribution of semi-major axes of surviving planets. (c) Distribution of eccentricity of surviving planets. (d) Distribution of inclination angle of surviving planets.

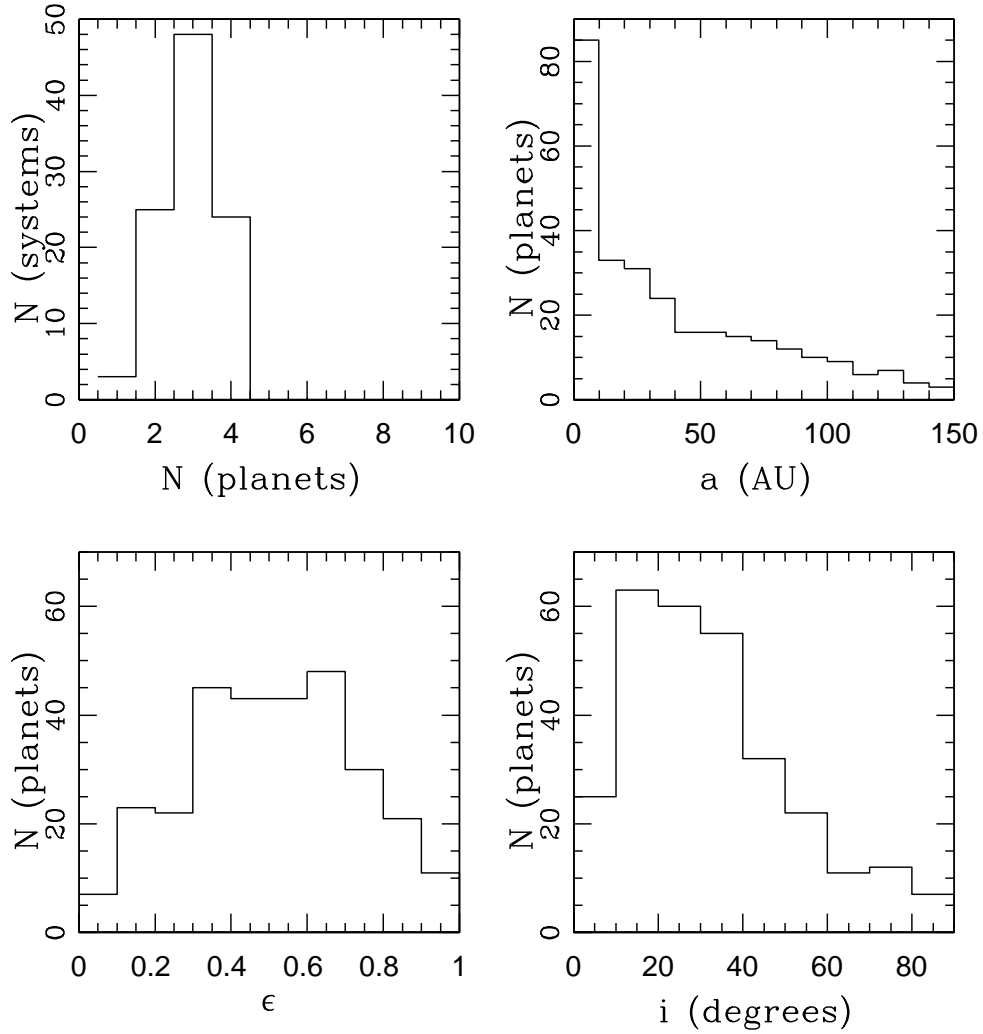


Fig. 4.— Characterization of solar system properties after 1 Myr of dynamical evolution – for planets with $m_P = 2 m_J$. The remaining planets from all $N = 100$ solar systems are folded together in these histograms. (a) Distribution of number of remaining planets. (b) Distribution of semi-major axes of surviving planets. (c) Distribution of eccentricity of surviving planets. (d) Distribution of inclination angle of surviving planets.

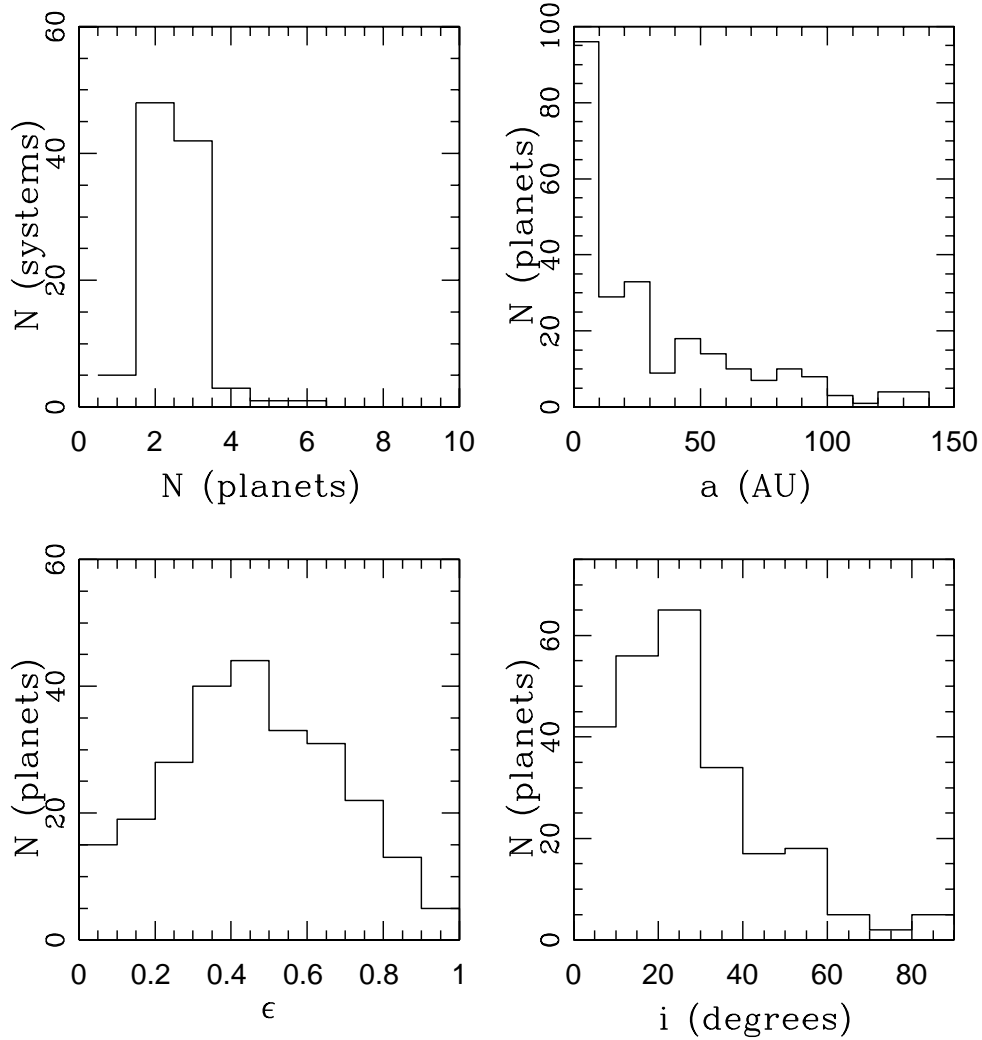


Fig. 5.— Characterization of solar system properties after 1 Myr of dynamical evolution – for planets with randomly chosen masses within the range $0 \leq m_P \leq 4m_J$. The remaining planets from all $N = 100$ solar systems are folded together in these histograms. (a) Distribution of number of remaining planets. (b) Distribution of semi-major axes of surviving planets. (c) Distribution of eccentricity of surviving planets. (d) Distribution of inclination angle of surviving planets.

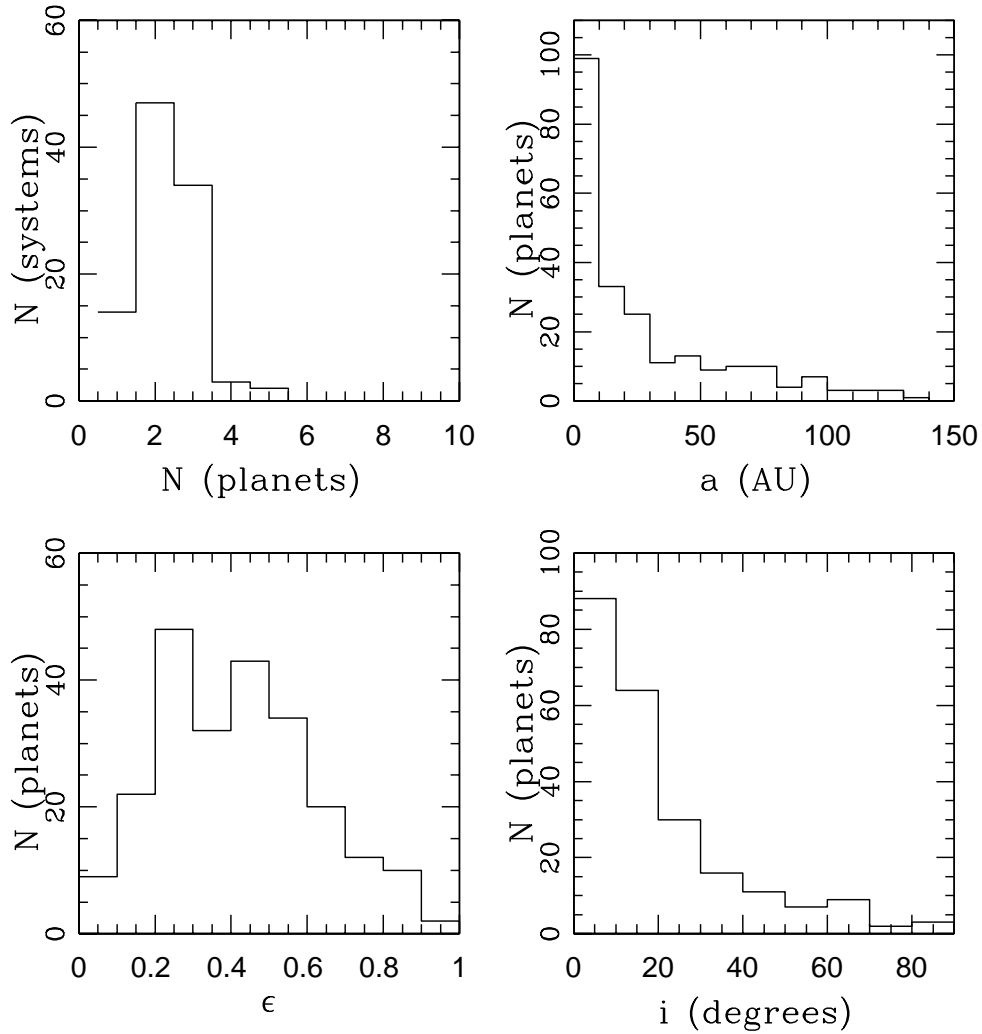


Fig. 6.— Characterization of solar system properties after 1 Myr of dynamical evolution – for planets with masses chosen randomly in $\log m$ within the range $-1 \leq \log_{10}[m_P/m_J] \leq 1$. The remaining planets from all $N = 100$ solar systems are folded together in these histograms. (a) Distribution of number of remaining planets. (b) Distribution of semi-major axes of surviving planets. (c) Distribution of eccentricity of surviving planets. (d) Distribution of inclination angle of surviving planets.

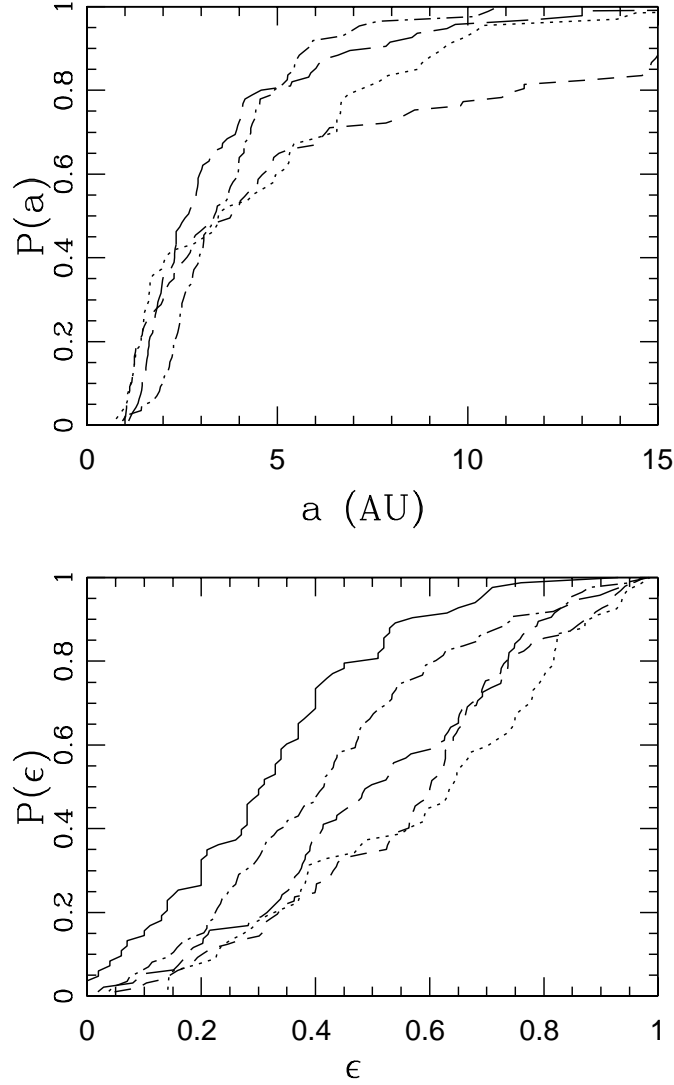


Fig. 7.— Orbital properties of the innermost planet. The upper panel shows the cumulative distribution for the semi-major axis of the innermost surviving planet. The dotted curve represents planets with $m_P = 1 m_J$; the dashed curve represents planets with $m_P = 2 m_J$; the long-dashed curve represents planets with randomly chosen masses in the range $0 \leq m_P \leq 4 m_J$; and dot-dashed curve represents planets with masses randomly chosen in $\log m$ in the range $-1 \leq \log_{10}[m_P/m_J] \leq 1$. The lower panel shows the corresponding distributions for the eccentricity of the innermost planet. Also shown is the cumulative distribution of eccentricity for the observed extra-solar planets (the subset of the sample with $a \leq 0.1$ AU).

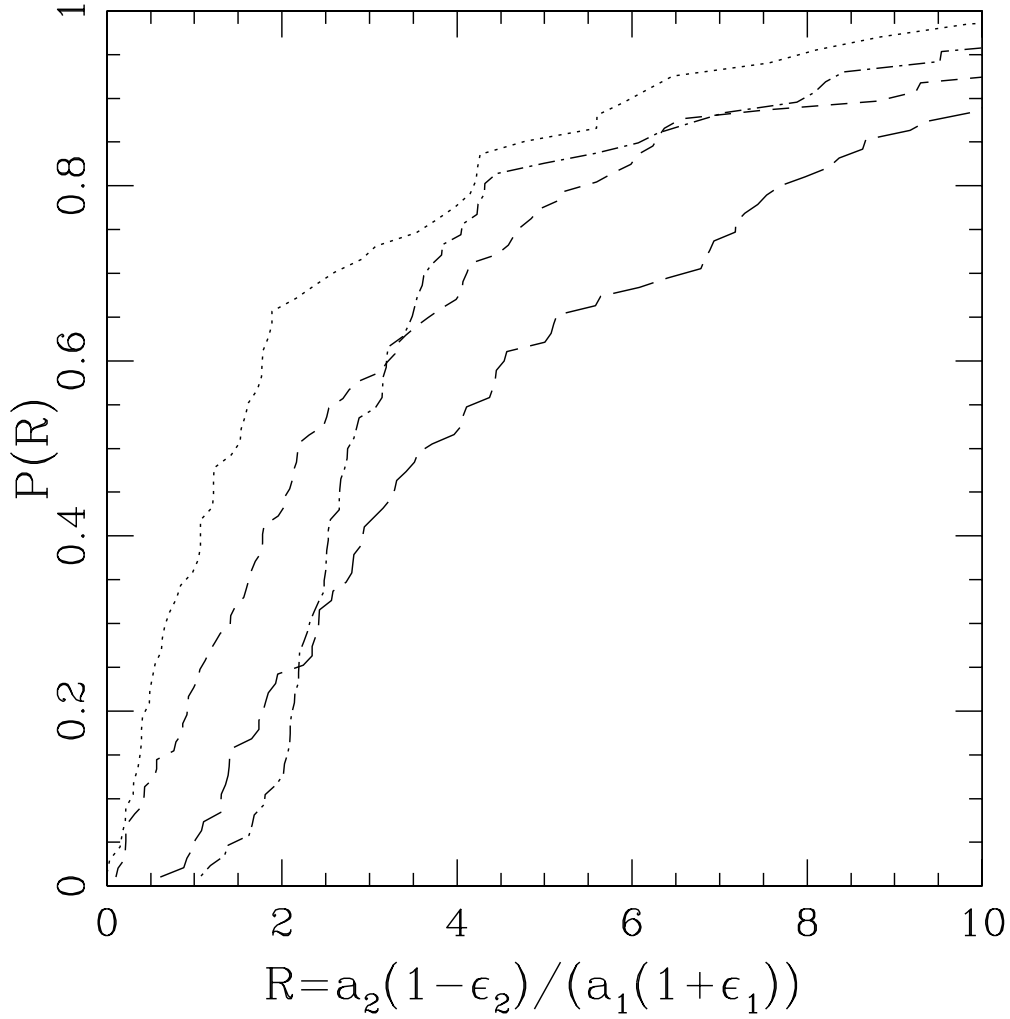


Fig. 8.— The cumulative distribution of for the ratio $R = a_2(1 - \epsilon_2)/(a_1(1 + \epsilon_1))$, i.e., the ratio of periastron of the second surviving planet to the apastron of the innermost surviving planet. The dotted curve represents planets with $m_P = 1 m_J$; the dashed curve represents planets with $m_P = 2 m_J$; the long-dashed curve represents planets with randomly chosen masses in the range $0 \leq m_P \leq 4m_J$; and dot-dashed curve represents planets with masses randomly chosen in $\log m$ in the range $-1 \leq \log_{10}[m_P/m_J] \leq 1$.

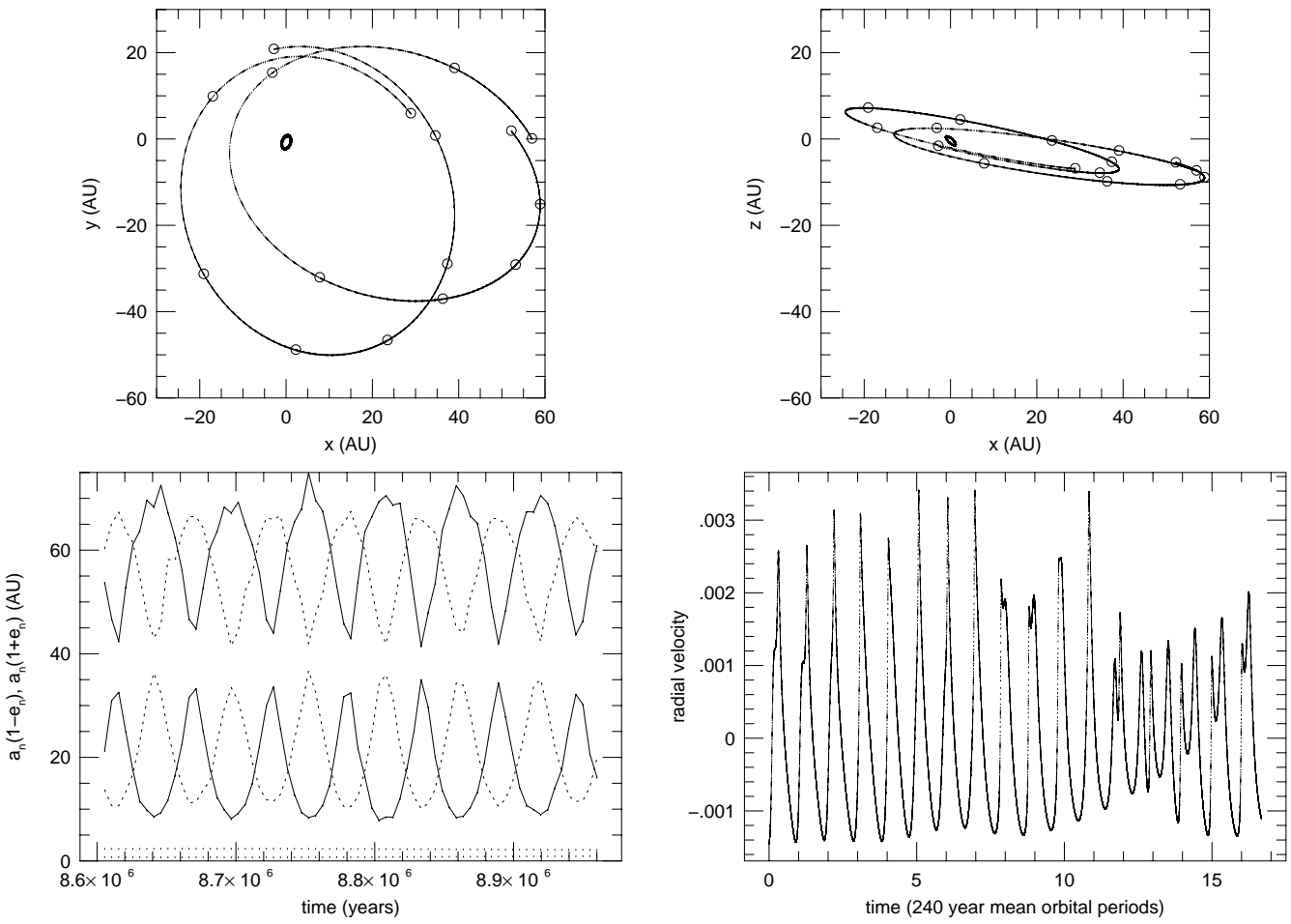


Fig. 9.— The eccentric 1:1 resonance. The scattering experiments often leave planets in resonant configurations, e.g., the 1:1 resonance depicted here. The lower left panel shows the history of the system during the final million years of the simulation by plotting $a(1 - e)$ and $a(1 + e)$ for each of the surviving planets. Sample trajectories of the planets are plotted in the upper two panels (the eight

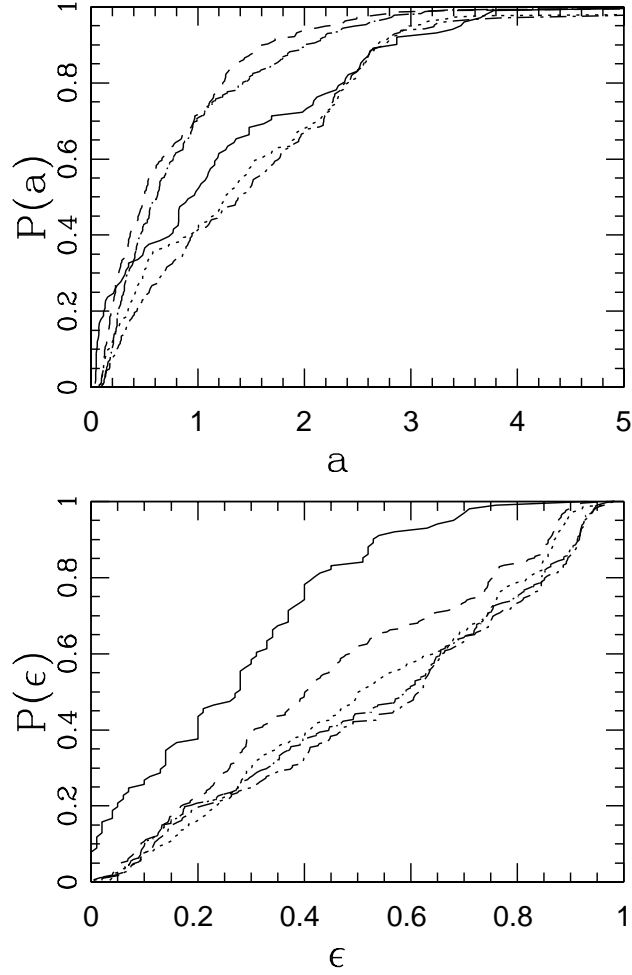


Fig. 10.— Distributions of orbital properties for the surviving planets in solar systems starting with two planets and a circumstellar disk that exerts tidal torques on the outer planet. The upper panel shows the cumulative distributions for the semi-major axis of the surviving planets. The lower panel shows the corresponding cumulative distributions for the eccentricity of the surviving planets. The solid curve depicts the distributions of the observed extrasolar planets. The distributions for the $\tau_{\text{ed}} = 1$ Myr simulations are shown as the long-dashed curves and the dotted curves (no evolution after the first planet is lost). The distributions for the $\tau_{\text{ed}} = 3$ Myr simulations are shown as the dot-dashed curves and the dashed curves (no evolution after the first planet is lost).

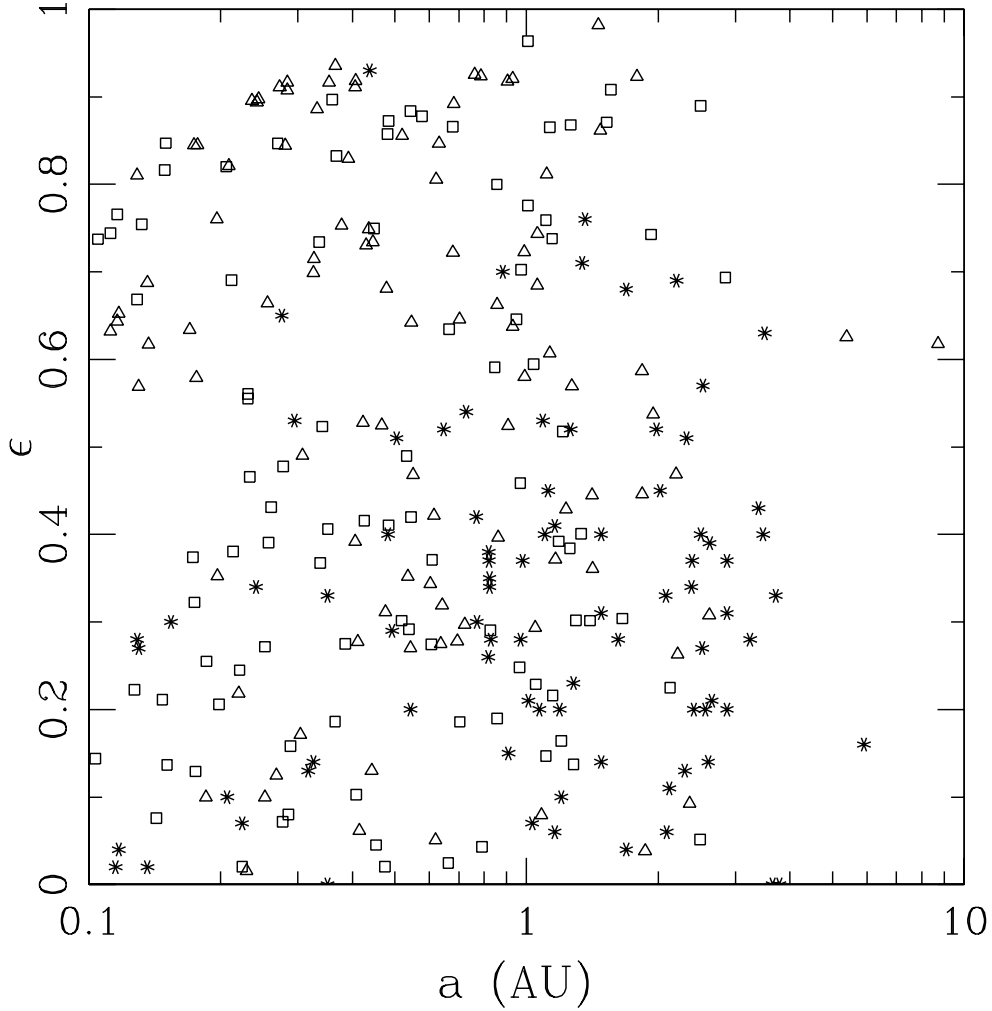


Fig. 11.— The $a - \epsilon$ plane for the observed population of extra-solar planets and the surviving planets in solar systems starting with two planets surrounded by a circumstellar disk. The star symbols represent the observed planetary orbits. The open triangles show the surviving planets for theoretical simulations using an eccentricity damping time scale $\tau_{\text{ed}} = 3$ Myr. The open squares show the surviving planets for simulations using $\tau_{\text{ed}} = 1$ Myr.